

An investigation of caldera-forming magma chambers using the timing of ignimbrite eruptions and pluton emplacement at the Mt. Aetna caldera complex

Matthew J. Zimmerer ^{a,*}, William C. McIntosh ^b

^a New Mexico Bureau of Geology and Mineral Resources, New Mexico Institute of Mining and Technology, Socorro, NM, 87801, USA

^b Earth and Environmental Sciences, New Mexico Bureau of Geology and Mineral Resources, New Mexico Institute of Mining and Technology, Socorro, NM, 87801, USA

ARTICLE INFO

Article history:

Received 22 March 2012

Accepted 10 August 2012

Available online 24 August 2012

Keywords:

⁴⁰Ar/³⁹Ar dating

U-Pb dating

caldera

pluton emplacement

silicic magmatism

ABSTRACT

The temporal and chemical relationships of volcanic and plutonic rocks exposed at the Mt. Aetna caldera complex, central Colorado, provide insight into the emplacement history of pre-, syn-, and postcaldera plutons and the origin of caldera-related silicic magmas. ⁴⁰Ar/³⁹Ar sanidine ages indicate the rhyolitic Wall Mountain Tuff erupted at 37.3 Ma. LA-ICP-MS U/Pb zircon ages of the compositionally zoned Mt. Princeton batholith, which has been interpreted by several previous studies to be the nonerupted, less-fractionated residuum of the Wall Mountain Tuff magma chamber, indicate that it was emplaced between 35.9 and 35.2 Ma during postcaldera magmatism. Nested within the Mt. Princeton batholith is the Mt. Aetna caldera. The dacitic Badger Creek Tuff erupted at 34.3 Ma during Mt. Aetna caldera collapse. The Badger Creek Tuff is deposited on some of the Mt. Princeton intrusive units, demonstrating that the Wall Mountain Tuff caldera was obliterated during exhumation and erosion prior to 34.3 Ma. Shortly after the Mt. Aetna caldera collapse, the intracaldera ignimbrite and caldera ring faults were intruded by magma that is compositionally and temporally similar to the Badger Creek Tuff, suggesting that these intrusions represent a nonerupted, geochemically equivalent portion of the magma chamber. Emplacement of postcaldera luecogranites at ~31 Ma caused localized thermal resetting of biotite and K-feldspar in older, adjacent intrusions. Most samples contain antecrustic zircon. Antecrustic zircon populations range from 38.8 to 33.6 Ma, indicating that open system magmatic processes operated throughout the history of the caldera complex. The temporal, chemical, and spatial relationships of plutonic and volcanic rocks at the Mt. Aetna caldera complex indicate that the majority of the exposed plutons were emplaced during pre- and/or postcaldera magmatism. None of the exposed plutons represent the less-fractionated, mafic residuum of either caldera-forming magma ignimbrite. This suggests that either the mafic roots of each caldera-forming magma chamber are not exposed or upper crustal in situ fractionation did not generate the caldera-forming silicic magmas.

© 2012 Elsevier B.V. All rights reserved.

1. Introduction

Caldera-related magmatism is a societally important geologic phenomenon. Caldera forming eruptions are arguably the most catastrophic geologic hazard (Francis and Oppenheimer, 2004; Miller and Wark, 2008; Self and Blake, 2008). Caldera systems are also potential sources of geothermal energy and economic ore deposits (Meyer and Foland, 1991; Hilton, 1996; Stimac et al., 2004; Klemm et al., 2008). Because of both the possible harm and potential benefit to society, caldera magmatism has been the focus of numerous studies. Understanding the rates and timescales of magma emplacement, the patterns of magma assembly, the sources of magmas, and eruption of subcaldera magmas is necessary for evaluating hazards at currently active caldera systems, assessing the geothermal potential of calderas, and developing genetic models to explain caldera-hosted ore deposits.

Many caldera-oriented studies have used the volcanic record to construct caldera evolution models and to infer the origin of silicic magmas (Lipman et al., 1978; Smith, 1979; Hildreth, 1981; Bachmann et al., 2002; de Silva and Gosnold, 2007). By nature, volcanic rocks represent a fragmental record of the entire magmatic history. Because of this, other studies have used plutonic rocks to understand the nature of silicic magmatism (Johnson and Lipman, 1988; Wiebe, 1994; Verplanck et al., 1999; Glazner et al., 2004). Processes such as magma emplacement, rejuvenation and modification of existing magma chambers, dike and sill emplacement, upwelling of magma during resurgence, and the duration of the waning stages of magmatism can be investigated using the plutonic record. However, understanding the relationships of plutonic processes with respect to volcanic processes, in the context of caldera-related silicic magmatism, is difficult in the absence of both records.

Extensive erosion and faulting related to the Rio Grande rift has exposed volcanic and plutonic rocks at the Mt. Aetna caldera complex (Fig. 1), Sawatch Range, central Colorado (Epis and Chapin, 1975; Shannon, 1988), providing an opportunity to examine caldera-related

* Corresponding author. Tel.: +1 575 835 5324.

E-mail address: mjz1983@nmt.edu (M.J. Zimmerer).

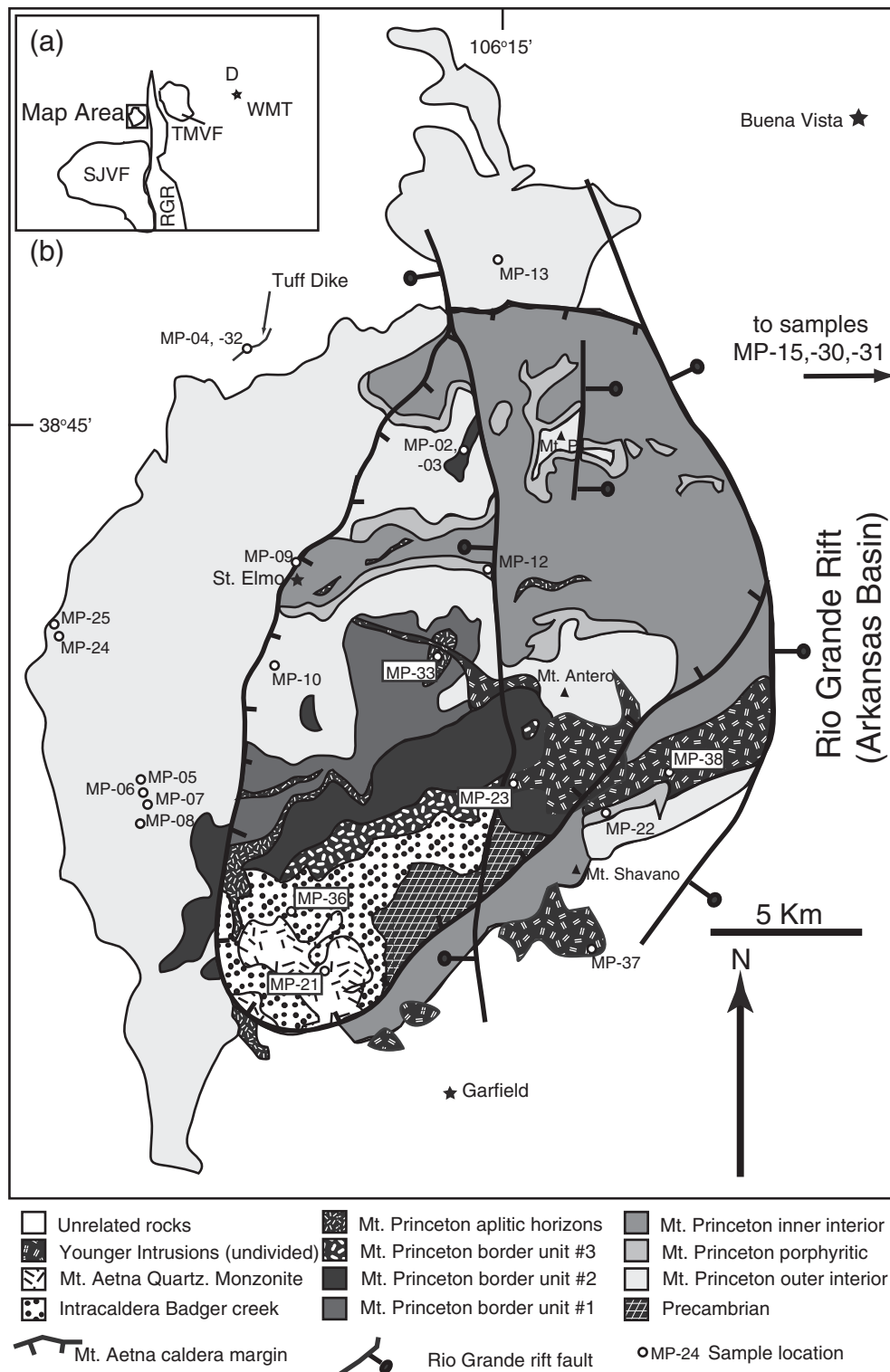


Fig. 1. (a) Map of Colorado showing the location of the San Juan Volcanic Field (SJVF), the Rio Grande Rift (RGR), the Thirty-nine Mile Volcanic Field (TMVF), and Denver (D). Star indicates most eastern outcrop of Wall Mountain Tuff (WMT). (b) Simplified geologic map of the Mt. Aetna caldera complex modified from Shannon (1988). Samples MP-15, 30, and 31 (not shown) are located in paleovalleys to the east. Unrelated rocks include Proterozoic granitoid and sedimentary rocks.

silicic magmatism. The specific goals of this work include: understanding emplacement histories and assembly patterns of pre-, syn-, and postcaldera plutons, establishing the volume, composition, and evolution of material that remains in the caldera-forming magma chamber after the collapse event, and determining the relative depth of silicic melt genesis. By comparing the temporal and chemical relationships

of caldera-related plutonic and volcanic rocks of the same caldera system, models for caldera magmatism can be assessed and modified.

This paper presents new $^{40}\text{Ar}/^{39}\text{Ar}$ and U/Pb ages of volcanic and plutonic rocks exposed at the Mt. Aetna caldera complex. $^{40}\text{Ar}/^{39}\text{Ar}$ dating constrains the timing of volcanic events and thermal evolution of the subcaldera batholith, and in absence of U/Pb ages, provides a

minimum age of pluton emplacement. Laser ablation-inductively coupled plasma-mass spectrometry (LA-ICP-MS) U/Pb zircon dating establishes the emplacement history of the exposed intrusive rocks. Additionally, the in-situ LA-ICP-MS technique allows for assessing zircon inheritance, which provides important information related to the source of magmas and detecting open-system magmatism. LA-ICP-MS U/Pb zircon ages are also compared to recently determined high-precision CA-TIMS U/Pb zircon ages (Mills, 2012). When relevant, existing geochemistry of volcanic and plutonic rocks exposed at the Mt. Aetna caldera complex (Campbell, 1994; Mills, 2012) is compared to $^{40}\text{Ar}/^{39}\text{Ar}$ and U/Pb ages to assess genetic relationships.

2. Evolving models for silicic caldera magmatism

The origin of silicic caldera magmas remains controversial (Glazner et al., 2004; Bachmann et al., 2007a; Lipman, 2007). During caldera collapse, a large volume ($10^2\text{--}10^4 \text{ km}^3$) of silicic magma is erupted from upper crustal magma chambers (Hildreth, 2004; Bachmann and Bergantz, 2008; Miller and Wark, 2008). Many studies have recognized that upper crustal silicic magmatism is ultimately driven by partial melting of the upper mantle and emplacement of basalt into the lower crust (Davies and Stevenson, 1992; Ulmer, 2001; Wood, 2004). Petrologic, geochemical, and experimental studies suggest two dominant, yet not necessarily exclusive processes for generating silicic melts from mafic magmas: in-situ differentiation via crystal fractionation (Bachmann and Bergantz, 2004; Walker et al., 2007; Bachmann and Bergantz, 2008) and partial melting of the crust (Dufek and Bergantz, 2005; Annen et al., 2006). Though both processes undoubtedly occur, disagreement exists regarding which process is dominant and the depth of silicic melt generation.

Several models propose that silicic melts are generated via in-situ fractionation of a magma chamber in the upper crust (Smith, 1979; Johnson, 1991; Bachmann et al., 2007a; Lipman, 2007; Walker et al., 2007). Early models suggested that basalt to rhyolite fractionation occurred in the upper crust (e.g., Smith, 1979). However, opponents of this early model cite problems with emplacing large volumes of dense basalt into the less-dense upper crust (e.g., Glazner, 1994; Dufek and Bergantz, 2005). Additionally, mafic magma emplaced into the relatively cold, upper crust may rapidly crystallize before crystal-liquid separation can occur. Recent studies have suggested that at least some differentiation of basalt occurs in the lower crust and that intermediate magmas are emplaced into the upper crust (Annen et al., 2006; de Silva and Gosnold, 2007), where they undergo further fractionation to silicic compositions (Miller and Miller, 2002; Bachmann et al., 2007a; Ulmer et al., 2007). According to this model, large-volume upper crustal caldera magma chambers fractionate to produce a compositionally zoned magma chamber, with a silica-rich (i.e., rhyolite) cap located above a silica-poor (i.e., andesite to dacite) residual crystal mush (Smith, 1979; Bachmann and Bergantz, 2004; Walker et al., 2007). The silicic cap is enriched in incompatible trace elements compared to the silica-poor, residual crystal mush (Deering and Bachmann, 2010). Most of the silicic cap is erupted during caldera collapse. Downward withdraw of material from the magma chamber terminates near or at the viscosity barrier between the silicic cap and the accumulated, residual crystal mush (Bacon and Drue, 1988; Hildreth, 2004). The residual crystal mush and the nonerupted silicic cap are preserved as plutons (Buddington, 1959; Shannon, 1988; Hildreth, 2004; Bachmann et al., 2007a; de Silva and Gosnold, 2007; Lipman, 2007). This model implies that a significant volume (3 to 10:1 intrusive extrusive ratio; White et al., 2006) of caldera-related plutonic rocks should be coeval with and geochemically complimentary (i.e., represent the less-fractionated mafic residuum of the magma chamber) to the associated ignimbrite (Smith, 1979; Bachmann et al., 2007a; de Silva and Gosnold, 2007).

Other studies suggest that silicic magmas are generated in deep crustal sources. Emplacement of mafic magma into the lower crust

causes partial melting of the country rocks. Magma derived from basal fractionation mix with partial melts of the lower crust and the hybrid, silicic magmas are emplaced into the upper crust (Eichelberger et al., 2000; Dufek and Bergantz, 2005; Annen et al., 2006; Quick et al., 2009). Some additional shallow fractionation may occur, but the degree of upper crustal fractionation is minor compared to that which occurs at deeper crustal levels. Assimilation of upper crustal material may also contribute to bulk composition trends of silicic magmas erupted during caldera collapse events (Knesel and Duffield, 2007; Lipman, 2007). During the caldera eruption, magma chambers can nearly completely drain because the highly viscous, less-fractionated residuum, if any, is located at deeper crustal levels (Coleman et al., 2004; Glazner et al., 2004; Annen et al., 2006). Accordingly, the nonerupted remnants of the caldera forming magma chamber represent a small percentage of the total shallow crustal intrusive suite and these coeval intrusions will have a similar geochemistry to the caldera-forming ignimbrite (Glazner et al., 2008; Mills et al., 2008; Tappa et al., 2011; Zimmerer and McIntosh, 2012). Furthermore, caldera-forming magma chambers are ephemeral features emplaced during high-magma-emplacement events (Glazner et al., 2004; Annen, 2009). Most plutons are emplaced during pre- or postcaldera magmatism when magmatic input is relatively low compared to during syncaldera magmatism (Lipman, 1984; Jellinek and DePaolo, 2003; Glazner et al., 2004; Tappa et al., 2011; Zimmerer and McIntosh, 2012).

3. Geology and previous studies of the Mt. Aetna caldera complex

Rocks exposed at the Mt. Aetna caldera complex (Fig. 1) and in adjacent paleovalleys represent the initiation of ignimbrite volcanism in the Southern Rocky Mountain volcanic field (McIntosh and Chapin, 2004; Lipman, 2007). During the Laramide flat-slab subduction of the Farallon plate, magmatism and volcanism migrated $>1000 \text{ km}$ to the east of the subduction trench. Following the decoupling of the Farallon plate from beneath the North America plate, the ignimbrite flare-up began in the western United States (Coney and Reynolds, 1977; Lawton and McMillan, 1999; Chapin et al., 2004). One of the largest erosional remnants of the ignimbrite flare-up is the Southern Rocky Mountain volcanic field, which includes over 30 calderas and corresponding ignimbrites (Lipman, 2007). Volcanism in the southern Rocky Mountains began in central Colorado and migrated to southwestern Colorado between 38 and 23 Ma (McIntosh and Chapin, 2004; Lipman, 2007; Lipman and McIntosh, 2008). Following the cessation of magmatism, large-scale faulting commenced during the initiation of the Rio Grande rift (Baldridge and Olsen, 1989). Faulting, uplift, and erosion related to the rift exposed the volcanic and plutonic rocks at the Mt. Aetna caldera complex (Shannon, 1988).

The magmatic evolution at the Mt. Aetna caldera complex consists of three temporally distinct stages. The Mt. Princeton batholith represents the oldest exposed magmatic event. Nested within the Mt. Princeton batholith is the younger Mt. Aetna caldera, the source of the Badger Creek Tuff. The youngest intrusions exposed intrusions are small volume luecogranites that cross cut many of the older intrusions.

The Mt. Princeton batholith has been suggested to be the nonerupted, residual crystal mush for the crystal-rich, low-SiO₂, rhyolitic, $>1000 \text{ km}^3$ Wall Mountain Tuff (Epis and Chapin, 1975; Shannon, 1988; Toulmin and Hammarstrom, 1990; Fridrich et al., 1998). The Mt. Princeton batholith is the largest mid-Tertiary intrusion in Colorado (Tweto, 1979; Shannon, 1988; McIntosh and Chapin, 2004). The batholith is composed of relatively homogeneous interior units (structurally lowest units; commonly referred to as the Mt. Princeton quartz monzonite) consisting of quartz monzonite and minor granite and the structurally highest, texturally diverse, more mafic border units (Shannon, 1988; Toulmin and Hammarstrom, 1990). Based on compositional zoning, continuous textural and compositional layers, and lack of cross cutting relationships, Shannon (1988) suggested the batholith was emplaced as a single

magma chamber which then differentiated to the various compositions. Numerous previous studies inferred that the Mt. Princeton batholith was the source of the Wall Mountain Tuff because 1) shallow fractionation models predict that large volumes of nonerupted mafic to intermediate residual mush remain in magma chambers after eruption and are preserved as plutons (Smith, 1979; Shannon, 1988; Toulmin and Hammarstrom, 1990; Bachmann and Bergantz, 2004; Bachmann et al., 2007a; Lipman, 2007; Bachmann and Bergantz, 2008), 2) paleovalleys that converge toward the Mt. Princeton batholith contain thick (~5–150 m) deposits of the Wall Mountain Tuff (Epis and Chapin, 1975; McIntosh and Chapin, 2004), and 3) the Wall Mountain Tuff and Mt. Princeton batholith have been reported to be similar in age (Shannon, 1988; Toulmin and Hammarstrom, 1990; Fridrich et al., 1998). Shannon (1988) highlighted the potential genetic relationship between some border units and the Wall Mountain Tuff, largely because of the presence of clinopyroxene in both units.

Several studies have investigated the temporal and chemical relationship between the Wall Mountain Tuff and Mt. Princeton batholith. Using the sanidine single-crystal laser-fusion technique, McIntosh and Chapin (2004) dated five samples of the Wall Mountain Tuff to obtain an age of 37.16 ± 0.09 Ma (all $^{40}\text{Ar}/^{39}\text{Ar}$ ages reported from previous studies are recalculated using FC-2 = 28.201 Ma; Kuiper et al., 2008). Toulmin and Hammarstrom (1990) report a $^{208}\text{Pb}/^{232}\text{Th}$ date of 36.6 Ma from the Mt. Princeton quartz monzonite, though the analytical errors are not provided. This study also reported hornblende $^{40}\text{Ar}/^{39}\text{Ar}$ incremental heating ages of 36.3 and 37.1 Ma. Neither analysis yielded a plateau; the ages are from the highest temperature steps and the authors speculate that excess ^{40}Ar may be present. Biotite $^{40}\text{Ar}/^{39}\text{Ar}$ ages of the Mt. Princeton interior units are between 35.0 and 34.7 Ma ($n = 4$) (McIntosh and Chapin, 2004). Differences in whole-rock, trace-element, and REE geochemistry led Campbell (1994) to suggest that the Mt. Princeton quartz monzonite is not the source for the Wall Mountain Tuff. The large range in ages from previous studies, incomplete sampling, and absence of any caldera features has prevented establishing a definitive relationship for the Wall Mountain Tuff and Mt. Princeton batholith.

Following emplacement of the Mt. Princeton batholith, the crystal-rich, dacitic, $> 250 \text{ km}^3$ Badger Creek Tuff erupted from the Mt. Aetna caldera during a series of numerous eruptions. The Antero Tuff, a regional ignimbrite that is interbedded with minor clastic sediments, also erupted during collapse of the Mt. Aetna caldera. The Antero Tuff has identical $^{40}\text{Ar}/^{39}\text{Ar}$ ages, mineral content, and paleomagnetic directions to the Badger Creek Tuff, and thus likely represents an early phase of the eruption (Shannon et al., 1987; McIntosh and Chapin, 2004). Because of the similarity of these two units and the likelihood that both tuffs erupted during the same Mt. Aetna caldera collapse event, for the remainder of this paper we will refer the Antero and Badger Creek Tuffs as simply the Badger Creek Tuff.

Evidence for the nested caldera includes the intracaldera Badger Creek Tuff, ring faults and shear zones, and a discontinuous ring dike that grades into a more massive quartz monzonite intrusion. The caldera formed during trap-door style collapse (Shannon et al., 1987; Toulmin and Hammarstrom, 1990). The greatest subsidence of the caldera floor occurred in the south, which is the only location of remaining intracaldera Badger Creek Tuff. At present erosional levels the majority of rocks within the Aetna ring faults are Mt. Princeton intrusive units that represent the eroded floor of the caldera. A quartz monzonite stock, which intrudes the intracaldera tuff, was originally interpreted as a resurgent pluton (Shannon, 1988). However, field relationships do not indicate any uplift of the intracaldera Badger Creek Tuff during the emplacement of the quartz monzonite stock (this study; Toulmin and Hammarstrom, 1990). Evidence to suggest the quartz monzonite intrudes the intracaldera Badger Creek Tuff include: a chilled-margin, lack of unconsolidated sediments, nonwelded tuff, or a vitrophyric zone between the tuff and intrusion, and the intrusion cross-cuts

megabreccia blocks. Based on similarities in geochemistry (whole-rock major and trace elements, REE distributions, and $^{87}\text{Sr}/^{86}\text{Sr}$ isotopic values), mineralogy, and fission-track and K/Ar ages, Shannon et al. (1987) and Campbell (1994) concluded that the ring dike and Mt. Aetna quartz monzonite pluton represent nonerupted Badger Creek equivalent magma that intruded into the intracaldera sequence shortly after caldera collapse. The Calico Mountain volcanic units and possibly several intrusive tuff dikes are the only record of pre-Mt. Aetna caldera volcanism (Shannon et al., 1987; Shannon, 1988).

The age relationships of the Calico Mountain volcanic units, Mt. Aetna quartz monzonite, ring dike, Badger Creek Tuff, and intrusive tuff dikes remains uncertain. Sanidine single-crystal laser-fusion analyses of the Badger Creek Tuff yielded an age of 34.25 ± 0.11 Ma. Hornblende and biotite $^{40}\text{Ar}/^{39}\text{Ar}$ analyses of the Mt. Aetna quartz monzonite yielded a weighted mean age of 34.51 ± 0.90 Ma. K-feldspar from the ring dike yielded an age of 34.57 ± 0.18 Ma, slightly older than the Badger Creek Tuff eruption age (McIntosh and Chapin, 2004). Fission-track ages of the intrusive tuff dikes are 33.4 and 33.7 Ma, but the associated errors are large and do not provide a definitive relationship to the Badger Creek Tuff (Shannon et al., 1987). Timing of Calico Mountain volcanism has not been determined, largely because of widespread alteration (Toulmin and Hammarstrom, 1990).

Following the Badger Creek Tuff eruption, numerous luecogranites were emplaced into the upper crust in the Mt. Aetna area (Shannon, 1988). The three largest luecogranitic intrusions are the Mt. Antero, California, and North Fork intrusions. Crosscutting relationships indicate that these intrusions represent the last stages of magmatism. Geochemistry suggests that these plutons are the most evolved melts in the complex (Shannon, 1988; Campbell, 1994; Mills, 2012) and are possibly related to Rio Grande rift bimodal magmatism (Shannon, 1988). Biotite and muscovite from the Mt. Antero granite yielded a weighted mean $^{40}\text{Ar}/^{39}\text{Ar}$ age of 29.97 ± 0.13 Ma (McIntosh and Chapin, 2004).

Several samples collected as part of this study were also dated using the CA-TIMS U/Pb method (Mills, 2012). These high-precision ages are compared to our LA-ICP-MS and $^{40}\text{Ar}/^{39}\text{Ar}$ ages. In order to avoid repetition, the CA-TIMS dating results are only briefly introduced here and are more thoroughly presented within the discussion. Samples of the Mt. Princeton batholith yielded ages that range from 35.82 ± 0.10 to 35.37 ± 0.09 Ma, whereas the Mt. Aetna caldera-related rocks yielded ages that range from 34.95 ± 0.04 to 34.47 ± 0.05 Ma.

4. Methods

Thirty-four volcanic and plutonic samples were collected as part of this study (see electronic supplementary appendix 1 for the location of dated samples). Four additional sanidine separates of the Wall Mountain Tuff were re-dated from McIntosh and Chapin (2004). From this suite, 38 mineral separates were dated using the $^{40}\text{Ar}/^{39}\text{Ar}$ method (8 sanidine, 18 biotite, and 12 K-feldspar separates) and 14 zircon separates were dated using the laser ablation-inductively coupled plasma-mass spectrometry (LA-ICP-MS) U/Pb technique.

Samples were collected from a variety of locations and units in order to obtain a representative sample suite of the caldera complex. Samples were taken of both the Mt. Princeton interior and border units. Sample MP-03 is especially important because it is the only Mt. Princeton intrusion that contains clinopyroxene, a mineral that is also present in the Wall Mountain Tuff (Shannon, 1988). Samples of the Mt. Princeton interior units were collected from both within and outside the Mt. Aetna ring dikes and faults to examine if caldera collapse affected the thermal history of the Mt. Princeton batholith. Alteration is common at the Mt. Aetna caldera complex. Only the most pristine samples were collected. Because intracaldera Wall Mountain Tuff is apparently completely eroded away, samples of outflow tuff were collected from paleovalleys to the east of the Sawatch Range. Both intracaldera and outflow facies of the Badger

Creek Tuff, as well as two samples of the tuff dike in the northwestern region of the field were also collected and dated.

Mineral separates were obtained using standard separating techniques. Following jaw crushing and disk milling, samples for $^{40}\text{Ar}/^{39}\text{Ar}$ analysis were processed using a Frantz magnetic separator and density liquids. Volcanic sanidine crystals were treated in HF acid to remove adhering glass. Samples intended for U/Pb zircon dating were processed using a Wilfley table to isolate dense minerals. Zircon separates were then processed using a Frantz magnetic separator and placed into lithium metatungstate and then methylene iodine heavy liquids to obtain zircon concentrates. Mineral concentrates were finally hand picked using a binocular microscope to obtain monomineralic separates.

LA-ICP-MS U/Pb zircon analyses were conducted at the Arizona Laserchron Center. Zircon separates and the 564 Ma Sri Lanka zircon standard were placed into pucks and imaged using a cathodoluminescence (CL) microscope. CL images were used to identify oscillatory zoning indicative of magmatic growth, potential inherited cores, and mineral inclusions. An excimer laser with a beam diameter of 30–35 μm was used to ablate the zircons. Zircon inheritance was assessed by comparing the ages of zircon interiors and rims. For each sample, at least 20 spots were analyzed. Isotopic ratios were measured using a GVI Isoprobe mass spectrometer. Data was reduced using the in-house program "Agecalc". Gehrels et al. (2008) provides a comprehensive description of analytical and data reduction procedures at the Arizona Laserchron Center.

$^{40}\text{Ar}/^{39}\text{Ar}$ analyses were performed at the New Mexico Geochronology Research Laboratory. Unknowns and the interlaboratory standard FC-2 (28.201 Ma; Kuiper et al., 2008) were placed into aluminum disks and irradiated in a known geometry. Argon was liberated from single crystals of sanidine using a CO₂ laser, whereas a double-vacuum Mo resistance furnace was used to incrementally heat plutonic K-feldspar and biotite. Following heating, sample gas was expanded into an all-metal extraction line and cleaned using SAES getter pumps. Isotopic ratios were measured using a MAP 215–50 noble gas mass spectrometer. A comprehensive description of operating and analytical procedures is provided in McIntosh et al. (2003).

5. Results

5.1. U/Pb Geochronology

Zircon separates from 14 samples were dated using the LA-ICP-MS technique. $^{206}\text{Pb}/^{238}\text{U}$ analyses were used to calculate ages, as recommended by Gehrels et al. (2008). A summary of the calculated $^{206}\text{Pb}/^{238}\text{U}$ zircon ages is provided in Table 1. U/Pb zircon data tables are located in electronic supplementary appendix 2.

LA-ICP-MS data was thoroughly examined in order to yield the most accurate and precise ages. Pb-loss in zircon was addressed using two methods. First, analyses that yielded $^{206}\text{Pb}/^{238}\text{U}$ ages with >10% uncertainty or >30% discordance were excluded from age calculations. Second, U concentrations were compared to the $^{206}\text{Pb}/^{238}\text{U}$ zircon ages. The samples did not display a correlation between high U concentration and $^{206}\text{Pb}/^{238}\text{U}$ age, which might be expected if radiation damage and Pb-loss were significant (Mattinson, 2005). However, some samples did display a relationship between low U concentration and imprecise, young ages. When confidently identified, these analyses were removed from the age calculations.

Weighted mean and UNMIX ages were calculated using Isoplot v3.7 (Ludwig, 2009). The range of U/Pb weighted mean ages for the suite of zircons is from 37.01 ± 0.27 to 30.75 ± 0.24 Ma. Some zircons contained Proterozoic cores. Ages obtained from Proterozoic cores were not used in the age calculations. MSWD (mean standard weighted deviates) values for the calculated U/Pb weighted mean ages range from 1.5 to 10.5. An MSWD of ~1 indicates that the scatter in the data is predicted by the analytical errors (Mahon, 1996). Elevated MSWD values of zircon ages have been attributed to the presence xenocrysts

and/or antecrysts, which are zircons that grew from an earlier episode of magmatism and recycled during later stages of magmatism (Miller et al., 2007).

To further investigate the high MSWD values, ages were recalculated using the UNMIX feature of Isoplot (Ludwig, 2009). The UNMIX age calculation, which is based on the methods of Cambridge and Compston (1994), determines statistically distinguishable age populations for samples containing individual ages that overlap within error. In order to determine the number of age populations, the program was run several times using an increasing number of components until the relative misfit parameter (a value that represents the inability of the number of populations to accurately describe the data) decreased to a constant value (i.e., adding more age populations does not improve the solution). UNMIX ages are located in Table 2. Fig. 2 contains the age probability density plots containing the UNMIX ages.

The UNMIX ages are preferred for geologic interpretation compared to the weighted mean ages. In general, most UNMIX ages correspond to major peaks, subpeaks, and/or distinct shoulders on the probability curves. This provides confidence in the ability of the method to distinguish multiple age populations from a complex distribution of relatively imprecise individual ages. UNMIX zircon ages range from 28.08 ± 0.79 to 39.19 ± 1.40 Ma. Typical precision for the calculated UNMIX ages is ~1–2% (2σ), though the total range in precision is from 0.48% to 5.3%. Between two and four distinguishable populations were calculated for each of the Mt. Aetna samples. The difference between UNMIX age populations, for any single sample, ranges from ~1 Ma to as much as ~5 Ma. Many samples yielded an UNMIX age population that was younger than the corresponding $^{40}\text{Ar}/^{39}\text{Ar}$ biotite age. Considering the relatively high temperature of zircon saturation (> 750 °C; Miller et al., 2003) compared to the closure temperature of biotite (~300–350 °C; Hodges, 1991), these 'young' UNMIX zircon age populations are problematic and thus were not used to make geologic interpretations. The cause of the 'young' UNMIX ages is not fully understood. Possibilities include Pb-loss not detected by the previously discussed methods and/or analyses of zircon domains that contain inclusions. The UNMIX feature also calculates the fraction of each age population. Though analysis of zircon interior-rim pairs is ideal, this was not always possible because of the large beam diameter, the presence of inclusions, scratches on the polished surface, and/or small size of the polished crystal faces. Therefore, the calculated fraction may not accurately represent the true fraction of each age population.

A robust crystallization age for sample MP-05, a Mt. Princeton unit, could not be confidently determined. The age probability diagram (Fig. 2h) contains a 34.26 ± 0.33 Ma major peak and a weakly defined, 36.32 ± 0.51 Ma shoulder. The age of the major peak is younger than the corresponding biotite age (35.54 ± 0.16 Ma) and therefore it not considered to accurately date the timing of zircon crystallization. Furthermore, it may suggest that Pb-loss is significant for this particular sample. The age of the shoulder is inconsistent with the $^{206}\text{Pb}/^{238}\text{U}$ and $^{40}\text{Ar}/^{39}\text{Ar}$ ages and field relationships of adjacent samples (i.e., MP-06, -07, and -08), which suggest emplacement at ~35 Ma. The UNMIX age of the shoulder may represent an antecrystic population.

5.2. $^{40}\text{Ar}/^{39}\text{Ar}$ Geochronology and Thermochronology

Thirty-eight mineral separates (8 sanidine, 18 biotite, and 12 K-feldspar) were dated using the $^{40}\text{Ar}/^{39}\text{Ar}$ technique. Table 2 summarizes the $^{40}\text{Ar}/^{39}\text{Ar}$ results. Ages were calculated using FC-2 = 28.201 (Kuiper et al., 2008) and $^{40}\text{K} \lambda_{\text{total}} = 5.463 \times 10^{-10} \text{ yr}^{-1}$ (Min et al., 2000). All $^{40}\text{Ar}/^{39}\text{Ar}$ data tables and associated plots are located in electronic supplementary appendix 3.

5.2.1. $^{40}\text{Ar}/^{39}\text{Ar}$ sanidine results

Eight sanidine separates were dated using the single-crystal laser-fusion (SCLF) analysis technique. For each sample, 15–30

Table 1

Summary of the LA-ICP-MS U/Pb ages of the Mt. Aetna caldera complex.

Sample	Unit	Wt. Mean Age (± 2) ¹	MSWD ²	UNMIX Ages (± 2) ³	Comments
Mt. Princeton Units					
MP-15	Wall Mountain Tuff	37.01 \pm 0.27	1.8	36.58 \pm 0.28 37.66 \pm 0.35	Oldest UNMIX age indistinguishable to Ar/Ar sanidine age; Contains abundant 1.4 Ga xenocrysts
MP-33	Mt. Princeton Border Unit	36.38 \pm 0.40	2.8	35.46 \pm 0.46 36.93 \pm 0.41 38.48 \pm 0.57	Oldest population from interiors of zircons; No clear correlation between the two youngest populations and analysis location
MP-03	Mt. Princeton Border Unit	36.21 \pm 0.28	1.5	35.21 \pm 0.51 36.48 \pm 0.26	Most mafic border unit; Contains 1.7 Ga xenocrysts
MP-07	Mt. Princeton Qtz. Monz.	35.92 \pm 0.25	1.6	35.37 \pm 0.35 36.27 \pm 0.24	Youngest zircon population agrees with CA-TIMS zircon age
MP-25	Mt. Princeton Qtz. Monz.	35.56 \pm 0.21	2.5	35.51 \pm 0.13 38.80 \pm 0.39	Located at PreCambrian contact, Contains 1.4 Ga xenocrysts
MP-10	Mt. Princeton Qtz. Monz.	35.20 \pm 0.50	10.5	34.41 \pm 0.21 35.62 \pm 0.50 36.40 \pm 0.29	No clear correlation between age and analysis location;
MP-08	Mt. Princeton Qtz. Monz.	35.12 \pm 0.30	1.5	34.72 \pm 0.36 35.85 \pm 0.48 39.19 \pm 1.40	Located outside Mt. Aetna collapse structure
MP-05	Mt. Princeton Qtz. Monz.	35.08 \pm 0.41	2.7	34.26 \pm 0.33 36.32 \pm 0.51	No correlation between age and analysis location; age probability curve does not contain subpeaks; Contains 1.6 Ga xenocrysts
MP-06	Mt. Princeton Qtz. Monz.	35.06 \pm 0.48	4.0	33.60 \pm 0.61 35.15 \pm 0.46 36.74 \pm 0.61 38.36 \pm 1.30	Most old ages are from cores and most young ages are from rims; No corresponding biotite age for comparison, but the 33 Ma population is anomalously young
Mt. Aetna Units					
MP-30	Badger Creek Tuff	34.69 \pm 0.33	6.5	33.66 \pm 0.33 34.83 \pm 0.22 35.60 \pm 0.31	Zircon crystallization age is slightly older than the sanidine Ar/Ar ages; Contains 1.4 Ga xenocrysts
MP-09	Mt. Aetna Ring Dike	35.01 \pm 0.41	10.0	33.54 \pm 0.50 34.68 \pm 0.26 36.28 \pm 0.26	Most zircon interiors yielded older ages, however some zircon yielded old rims with younger cores; Contains 1.4 and 1.7 Ga xenocrysts
MP-21	Mt. Aetna Qtz. Monz.	36.40 \pm 0.35	7.3	32.05 \pm 1.70 34.36 \pm 0.59 35.82 \pm 0.24 37.17 \pm 0.1	Youngest ages related to low U conc.; Most old ages are analyses of zircon interiors and most young ages are of zircon exteriors
Younger Plutons					
MP-37	North Fork Leucogranite	31.29 \pm 0.29	2.7	28.08 \pm 0.79 31.37 \pm 0.18	No zircon inheritance
MP-38	California Leucogranite	30.75 \pm 0.24	2.4	30.75 \pm 0.15 33.59 \pm 0.52	No zircon inheritance; Youngest exposed pluton

1 – Weighted mean age calculated relative to Sri Lanka Zircon (564 ± 4 Ma), ^{238}U and ^{235}U decay constants equal to 9.8485×10^{-10} and 1.55125×10^{-10} yr $^{-1}$, and $^{238}\text{U}/^{235}\text{U}$ equal to 137.88. Error only includes analytical measurements. Addition of external errors (e.g. decay constant, age of standard, fractionation factor, and common Pb correction) typically increases the uncertainty by ~1% of the age.

2 – Mean Standard Weighted Deviants.

3 – UNMIX ages calculated using the same systematic as the weighted mean ages. UNMIX ages in italics indicate that the youngest zircon age population is younger than the biotite age for that sample. UNMIX ages in bold are the preferred zircon crystallization ages for the units. For intrusive rocks, this age is the best estimate of the emplacement age. The older zircon populations are likely antecrysts. See text for additional explanations.

crystals were analyzed. Analyses of xenocrystic sanidine or plagioclase grains were not used in the age calculations. Analyses with radiogenic yields <95% or anomalously large errors were also excluded from the age calculation. MSWD values for the SCLF analyses range from 0.95 to 6.76. The high MSWD values for some samples indicate scatter in the data that is not attributed solely to analytical error.

Five samples were dated from the Wall Mountain Tuff. Sample ages range from 37.10 ± 0.10 to 37.34 ± 0.06 Ma and yield a weighted mean age of 37.25 ± 0.08 Ma (MSWD = 1.26) (Fig. 3). This age is interpreted as an accurate eruption age for this ignimbrite. The MSWD of ~1 indicates a near Gaussian distribution of ages. Two Wall Mountain Tuff

samples contained xenocrysts. Sample NM-1416 contained abundant xenocrysts with ages ranging from 38 to 375 Ma. Sample MP-15 contained two 37.7 Ma xenocrysts. Xenocrystic sanidine were probably incorporated from vent walls or entrained into the ignimbrite as it flowed. The weighted mean age of the Wall Mountain Tuff is indistinguishable to the published age of 37.16 ± 0.09 Ma (McIntosh and Chapin, 2004).

Three sanidine samples were dated to obtain an age for the Badger Creek Tuff. Ages range from 34.24 ± 0.05 to 34.28 ± 0.06 and yield a weighted mean age of 34.26 ± 0.06 Ma (MSWD = 0.13) (Fig. 3). The weighted mean age is interpreted to be the eruption age of the ignimbrite and the timing of Mt. Aetna caldera collapse. The low MSWD

Table 2Summary of $^{40}\text{Ar}/^{39}\text{Ar}$ ages for the Mt. Aetna caldera complex.

Caldera Stage	Sample	Unit	Mineral ¹	Age calculation method ²	Age (Ma) ³	Error ⁴
Wall Mountain Tuff						
	MP-15	Outflow	san	ideo.	37.34	0.06
	MP-15-HF	Outflow	bt	plt.	37.24	0.11
	MP-15	Outflow	bt	plt.	37.51	0.09
	NM-1152	Outflow	san	ideo.	37.24	0.08
	NM-1307	Outflow	san	ideo.	37.23	0.12
	NM-531	Outflow	san	ideo.	37.20	0.07
	NM-1416	Outflow	san	ideo.	37.10	0.10
Mt. Princeton Border Unit Plutonism						
	MP-03	Mt. Princeton Border Unit 2	bt	plt.	35.78	0.11
	MP-02	Mt. Princeton Border Unit 2	bt	int. (rcl.)	35.72	0.16
Mt. Princeton Interior Unit Plutonism						
	MP-24	Outer interior Qtz. Monz.	bt	plt.	35.56	0.11
	MP-24	Outer interior Qtz. Monz.	kspars	plt.	35.27	0.11
	MP-05	Outer interior Qtz. Monz.	bt	int.	35.54	0.16
	MP-05	Outer interior Qtz. Monz.	kspars	int. (alt.)	35.06	0.34
	MP-25	Outer interior Qtz. Monz.	bt	int. (rcl.)	35.46	0.16
	MP-25	Outer interior Qtz. Monz.	kspars	plt.	35.10	0.08
	MP-10	Outer interior Qtz. Monz.	bt	int. (rcl.)	35.33	0.16
	MP-10	Outer interior Qtz. Monz.	kspars	plt. (a.l.)	33.33	0.11
	MP-08	Outer interior Qtz. Monz.	bt	int. (rcl.)	35.28	0.19
	MP-08	Outer interior Qtz. Monz.	kspars	plt.	35.57	0.19
	MP-07	Outer interior Qtz. Monz.	bt	plt.	35.23	0.09
	MP-13	Outer interior Qtz. Monz.	bt	int. (rcl.)	34.37	0.18
	MP-13	Outer interior Qtz. Monz.	kspars	int. (a.l.)	34.23	0.17
	MP-12	Porphyritic Qtz. Monz.	bt	int. (rcl)	31.49	0.18
	MP-12	Porphyritic Qtz. Monz.	kspars	int. (a.l.)	27.99	0.14
	MP-22	Porphyritic Qtz. Monz.	bt	int. (rcl.)	30.80	0.12
Pre-Badger Creek volcanism						
	MP-04	Tuff dike	bt	int. (xeno.)	37.54	0.17
	MP-32	Tuff dike	bt	int. (xeno.)	62.37	0.17
	MP-32	Tuff dike	bt	ideo.	34.53	0.12
Badger Creek Tuff						
	MP-30	Outflow	san	ideo.	34.28	0.06
	MP-30	Outflow	bt	int. (alt; xeno.)	38.55	0.43
	MP-31	Outflow	san	ideo.	34.26	0.06
	MP-31	Outflow	bt	int. (alt, xeno.)	35.01	0.49
	MP-36	Intracaldera	san	ideo.	34.24	0.05
Mt. Aetna Intrusions						
	MP-21	Mt. Aetna Qtz. Monz.	kspars	int. (a.l.)	33.93	0.09
	MP-09	Ring Dike	kspars	int. (exc., xeno.)	40.02	0.18
Younger Plutonism						
	MP-38	California Luecogranite	bt	plt.	30.07	0.08
	MP-38	California Luecogranite	kspars	int. (a.l.)	26.45	0.12
	MP-37	North Fork Luecogranite	bt int.	29.65	0.09	
	MP-37	North Fork Luecogranite	kspars	int. (a.l.)	29.02	0.13
	MP-23	Mt. Antero Luecogranite	kspars	int. (a.l.)	28.18	0.13

1 - san (sanidine); bt (biotite); kspars (K-feldspar).

2 - ideo. (ideogram); plt. (plateau age); int. (Integrated age); rcl. (recoil); alt. (alteration); a.l. (argon loss via reheating); xc. (xenocrysts); exc. (excess argon).

3 - Age calculated relative to FC-2 equal to 28.201 Ma (Kuiper et al., 2008).

4 - Error (2σ) includes uncertainty in J and irradiation parameters. Error does not include uncertainty in ^{40}K decay constant.

value is interpreted as an artifact of the small number of samples used to calculate the weighted mean age rather than an overestimation of errors. Though the newly calculated age is indistinguishable to the published age for the Badger Creek Tuff, 34.25 ± 0.11 Ma (McIntosh and Chapin, 2004), the error is slightly more precise.

5.2.2. $^{40}\text{Ar}/^{39}\text{Ar}$ biotite results

Eighteen biotite separates were dated to determine the timing of volcanic eruptions and plutonic thermal histories. Six representative age spectra are shown in Fig. 4. The total range in ages is 62.37 ± 0.17 to 29.65 ± 0.09 Ma. For age spectra that contained a plateau, the age was calculated by weighting each step of the plateau by the inverse variance. A plateau is defined as three consecutive steps that overlap in error at 2σ and contain $\geq 50\%$ of the ^{39}Ar released (Fleck et al., 1977). For analyses that did not yield a plateau, the age was calculated by using the integrated age of all the steps.

Biotite age spectra display a variety of complexity related to the degree of alteration, recoil, and/or possible xenocrystic contamination. Six

out of eighteen biotite analyses yielded a plateau. For these six samples, the plateau comprises ~50 to 100% of the total ^{39}Ar released (e.g., Fig. 4a-d). For intrusive samples, the biotite plateau age determines the timing of cooling to ~ 300 – 350 °C (Hodges, 1991). The only volcanic biotite analyses that yielded a plateau were from the Wall Mountain Tuff. Two aliquots of the Wall Mountain Tuff biotite were analyzed, one sample pretreated in HF and the other untreated. The untreated biotite yielded a plateau of 37.51 ± 0.09 , which is statistically older than the corresponding sanidine age of 37.34 ± 0.06 . The HF treated biotite from the Wall Mountain Tuff yielded an age of 37.24 ± 0.11 (Fig. 4b), which is statistically indistinguishable to the corresponding sanidine age. HF treatment likely removed adhering glass or inclusions that contain minor amounts of excess ^{40}Ar .

Twelve biotite analyses did not yield a plateau. For most of these samples, the ages of steps gradually increase during the first 40% of ^{39}Ar released and then subsequently decrease (e.g., Fig. 4e and f). The overall ^{39}Ar release pattern is characteristic of ^{39}Ar recoil in some altered samples (Lo and Onstott, 1989). Typical K₂O values for

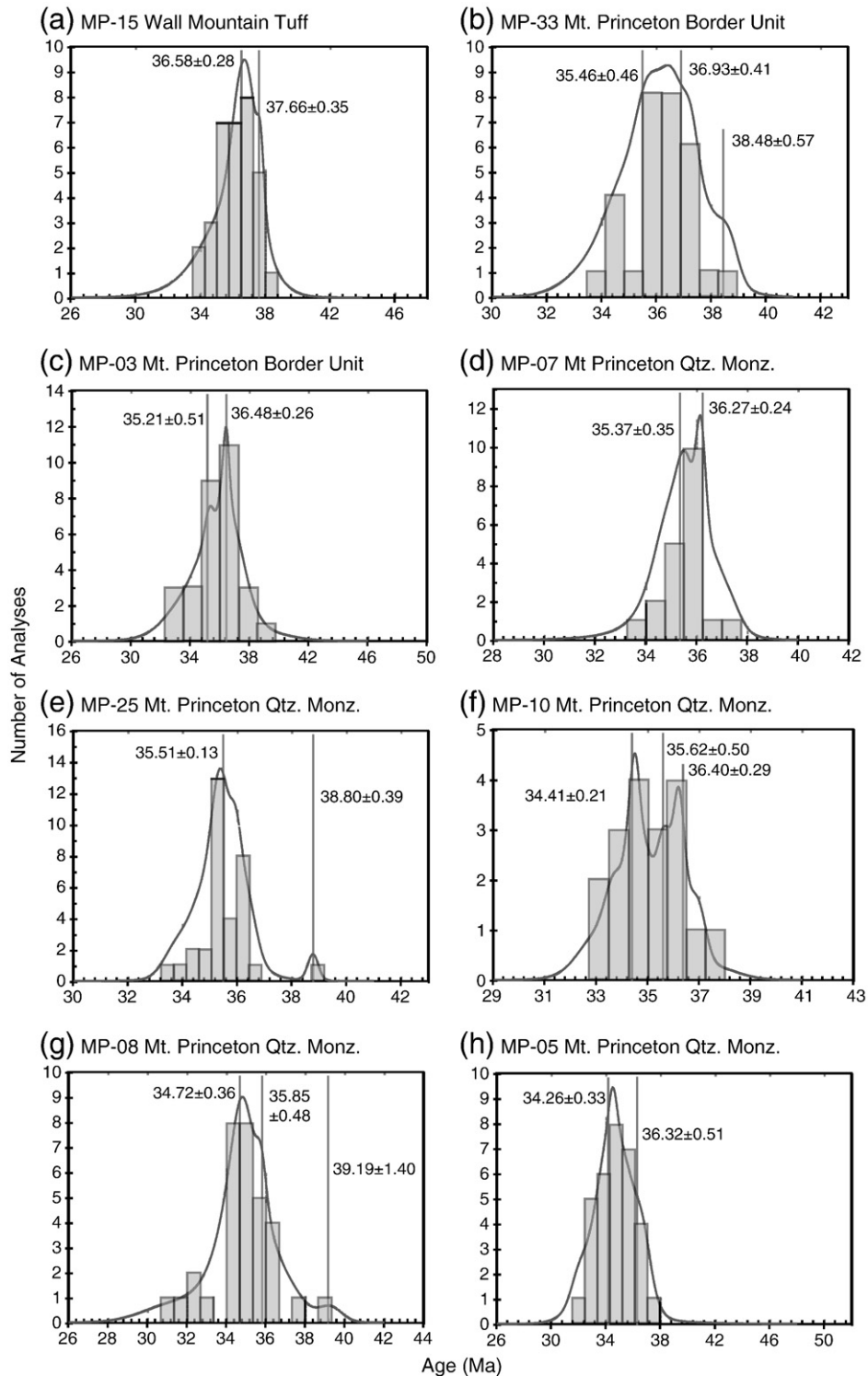


Fig. 2. Age probability density plots of the Mt. Aetna caldera complex LA-ICP-MS U/Pb zircon analyses. Vertical gray lines on the probability density curves represent UNMIX ages, which were calculated in Isoplot (Ludwig, 2009) using the methods of Sambridge and Compston (1994). All errors reported at 2 σ .

pristine biotite are 8–10% (McDougall and Harrison, 1999). K₂O values for the disturbed biotite spectra are 5–6%, which suggests alteration and probable ³⁹Ar recoil. For these samples, the integrated age is interpreted to be the most accurate age (Heizler et al., 1988; Lo and Onstott, 1989). Though the age spectra for samples MP-30 and MP-31 (i.e., Badger Creek outflow sheet) have a broad hump shape, the integrated age is 1–3 Ma older than the corresponding sanidine age. This suggests that some ³⁹Ar may have been recoiled out of the

sample, thereby increasing the age. Alternatively, some of the biotite crystals that were dated in the bulk analysis may be xenocrysts.

Two biotite separates (MP-04 and MP-32), both from the northwestern intrusive tuff dike, were dated to determine the eruption age of the tuff and potentially to correlate it to the Badger Creek Tuff. The bulk separates were incrementally heated, one using the resistance furnace and the other with a defocused CO₂ laser (Fig. 5a). Though both samples display initially old steps that gradually decrease in age during

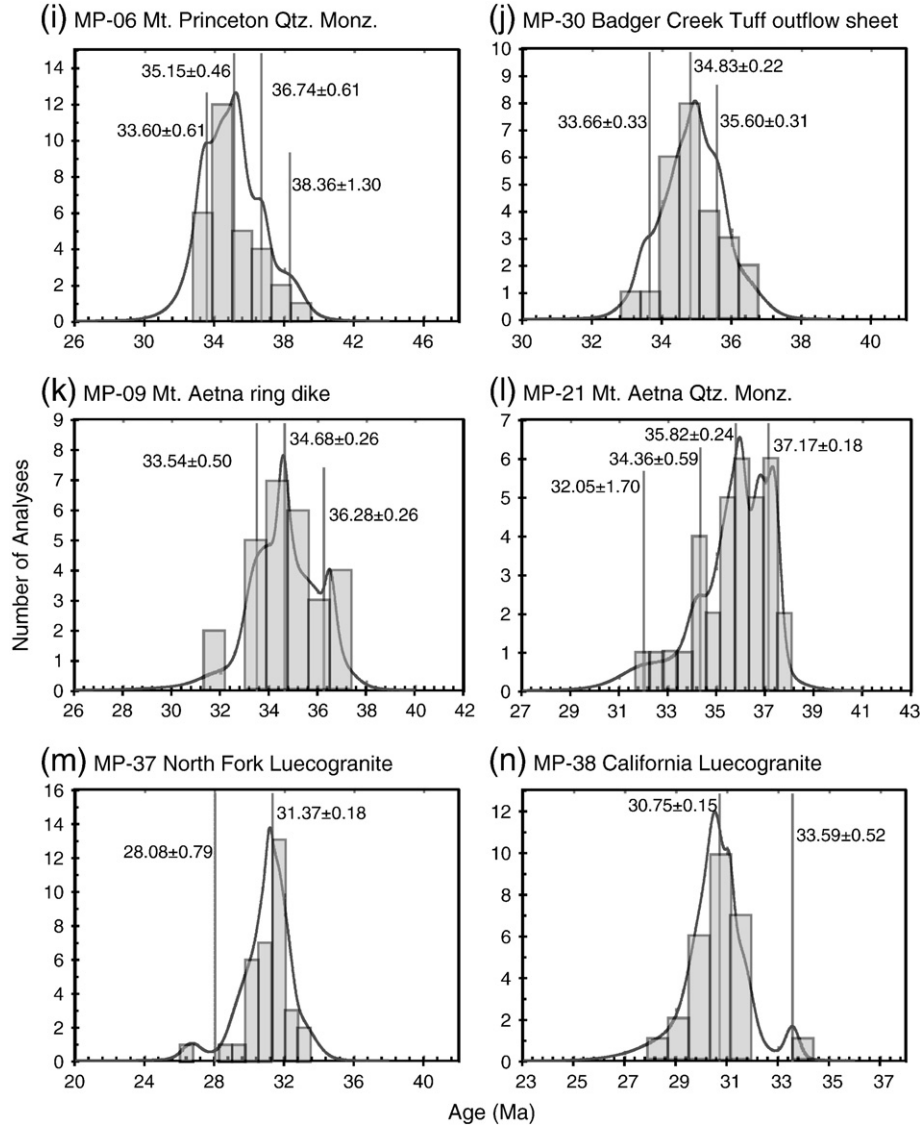


Fig. 2. (continued).

the experiment, the pattern is far more pronounced for sample MP-32. To assess xenocrystic contamination, 15 aliquots of 5–10 crystals were fused using the CO₂ laser. The multiple-crystal laser-fusion analysis yielded a weighted mean age of 34.53±0.12 Ma (MSWD=2.07, Fig. 5b). No aliquots were anomalously old, which suggests that xenocrysts, if present, constitute a very small percentage (e.g., <1%) of the total population. The laser-fusion weighted mean age is interpreted to be an accurate emplacement age for the tuff dike.

5.2.3. ⁴⁰Ar/³⁹Ar K-feldspar results and MDD thermal histories

Twelve plutonic K-feldspar separates were dated to constrain the 300–150 °C thermal history of the intrusive units (Lovera et al., 1989). Age spectra are plotted in Fig. 6 and ages are reported in Table 2. Step-heating schedules included isothermal duplicates steps to assess excess ⁴⁰Ar in fluid inclusions (Harrison et al., 1994). Seven samples were modeled in accordance to the multiple diffusion domain (MDD) theory (Lovera et al., 1991, 1997) using the methods of Sanders and Heizler (2005). Samples that yielded flat ³⁹Ar release profiles were not modeled because the geometry of the spectra indicates rapid cooling through the K-feldspar closure temperatures. Likewise, samples that yielded anomalous results were not modeled. For age spectra that contained argon loss profiles, two thermal histories were generated. Monotonic cooling histories (Fig. 7) only allow

for cooling from initially high temperatures, whereas unconstrained thermal histories (Fig. 8) allow for reheating events. Additional MDD figures are provided in electronic supplementary appendix 4.

Four of the twelve samples yielded nearly flat age spectra (MP-05, -08, -24, -25; Fig. 6 a, b, i, and j). The initial 10–25% of the age spectrum is characterized by discordant contiguous steps. This portion of the age spectra also contains oscillating radiogenic yields and K/Ca values. The initial discordance is probably related to fluid inclusions that contain excess and/or atmospheric ⁴⁰Ar (Harrison et al., 1994). The plateau segment for these samples indicates the timing of cooling. One sample, MP-05 (Fig. 6a), did not yield a plateau, but the age spectrum is nearly flat. For this sample, the integrated age is interpreted to be the timing of cooling.

Seven K-feldspar age spectra are characterized by argon loss profiles indicative of slow cooling and/or reheating events (Gillespie et al., 1982; Heizler et al., 1988; Lovera et al., 1989). The age gradients observed in the K-feldspar age spectra range from ~1–2 Ma to as much as 8–10 Ma. Sample MP-13 (Fig. 6f) has the smallest age gradient. Both the monotonic and unconstrained thermal histories indicate rapid cooling between 34 and 32 Ma (Figs. 7c and 8c). Using Al-in-hornblende geobarometry, Hammarstrom and Zen (1986) concluded the Mt. Princeton batholith was emplaced at 1 kbar or ~3 km. Based on the depth of emplacement, the large age gradients observed

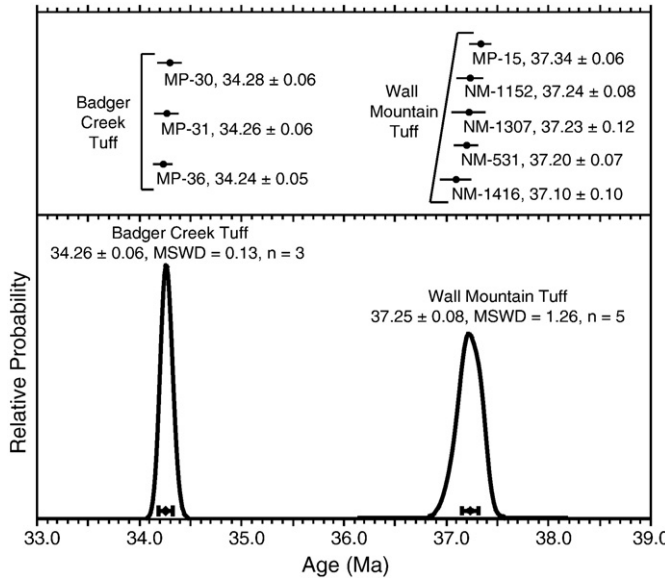


Fig. 3. Summary ideogram of Wall Mountain and Badger Creek Tuff sanidine separates dated as part of this study. Each data point represents the weighted mean age calculated from sanidine single-crystal laser-fusion analyses. All errors are reported at 2 σ .

in the remainder of the K-feldspar spectra are not interpreted to be the result of protracted cooling in the very shallow upper crust. Instead, the argon loss profiles are attributed to reheating events during protracted magmatism (see discussion for more detail).

The K-feldspar from the Mt. Aetna ring dike, MP-09 (Fig. 6c), yielded anomalous results. The initial part of the age spectrum is characterized by oscillating ages of isothermal duplicate steps, which are indicative of excess ^{40}Ar . At ~20% ^{39}Ar released, the ages

of steps gradually climb to ~40 Ma, which is ~6 Ma older than the intracaldera Badger Creek Tuff that the unit intrudes. The anomalous results may be related to ^{40}Ar in the largest domains (Foster et al., 1990) or xenocrystic contamination.

6. Discussion

6.1. Interpretation of zircon probability diagrams and UNMIX ages

Several guidelines were used to interpret the zircon age probability diagrams and the UNMIX age results. Age probability plots reveal numerous intra-sample U/Pb zircon age populations. As previously discussed, some samples contain UNMIX age populations that are younger than the corresponding $^{40}\text{Ar}/^{39}\text{Ar}$ biotite age. These ages were not used for any geologic interpretation. After discarding these 'young' populations, samples commonly contained UNMIX age populations separated by more than 1 Ma. Intra-sample UNMIX age populations are interpreted to be related to recycling of zircons (i.e., antecrysts; Miller et al., 2007) during protracted magmatism, rather than extended crystallization of a single pulse of magma.

If extended crystallization is called upon to explain intra-sample zircon age variation it requires that many samples remained near the solidus for prolonged periods (i.e., ~1–3 Ma). For example, MP-25 is located within several meters of the Precambrian contact. UNMIX ages for this particular sample are 35.5 and 38.8 Ma, which, in the framework of extended crystallization, suggests a 3.3 Ma period at or above the solidus. This explanation seems unlikely considering the close proximity to relatively cool country rock and the shallow depth of emplacement (Toulmin and Hammarstrom, 1990). For this particular sample the oldest population is defined by a single analysis, which does not sufficiently support an interpretation that the age variation represents the rejuvenation of the 38.8 Ma mush during a period of 3.5 Ma magmatism. A more plausible explanation is that range of UNMIX ages, within any given sample, is related to assimilation of

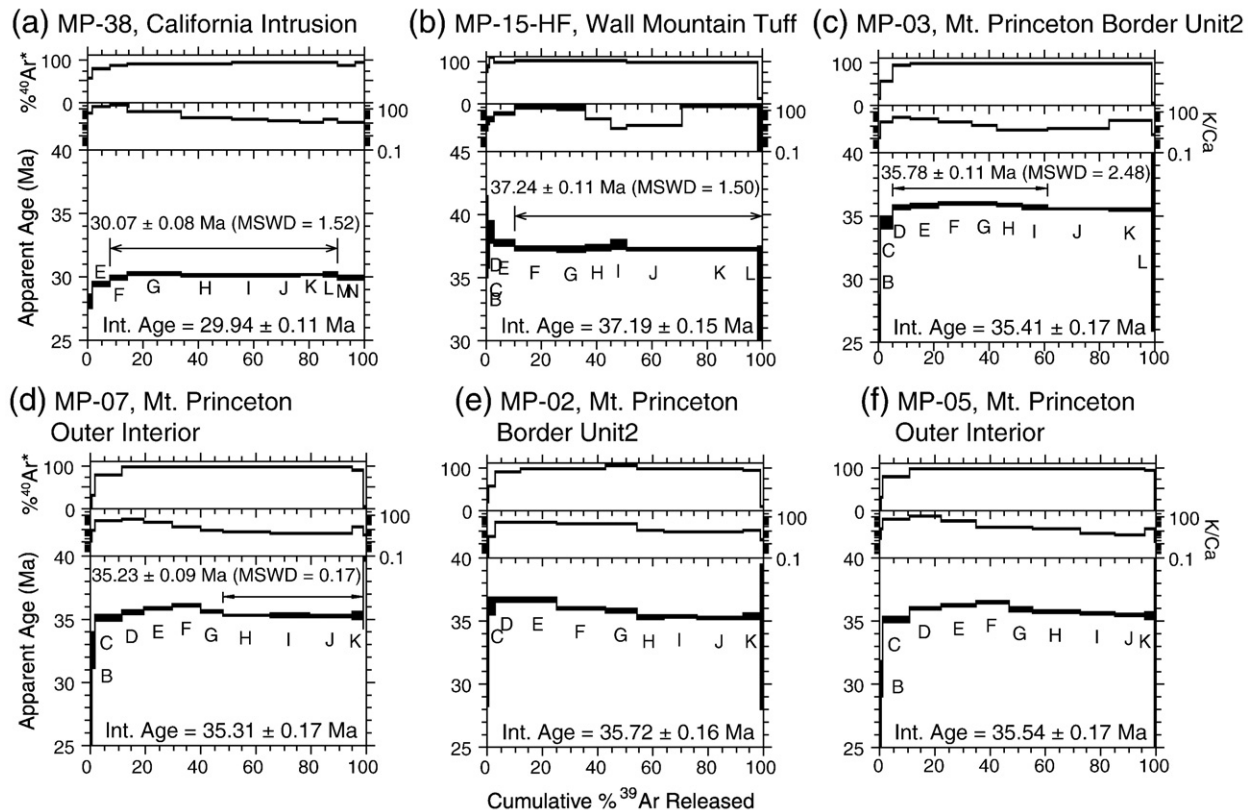


Fig. 4. Six representative age spectra for the Mt. Aetna caldera complex biotite separates. Auxiliary plots include K/Ca and radiogenic yield (% $^{40}\text{Ar}^*$). All errors are reported at 2 σ .

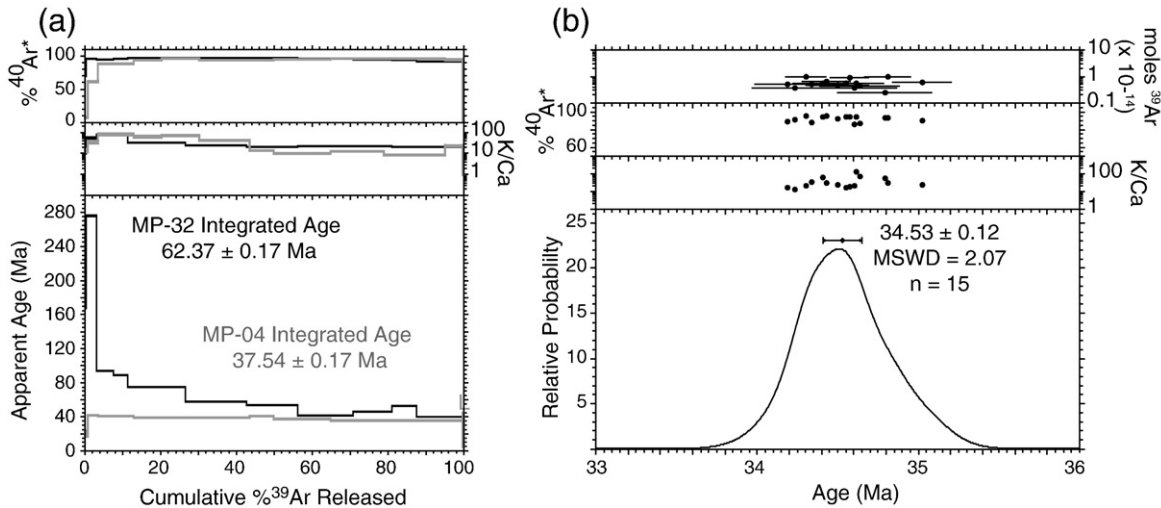


Fig. 5. $^{40}\text{Ar}/^{39}\text{Ar}$ analyses of biotite from the intrusive tuff dike. (a) Age spectra of the incrementally-heated biotite separates. MP-04 was step-heated using the double-vacuum Mo resistance furnace, whereas MP-32 was step-heated using the CO_2 laser. (b) Ideogram of the multiple-crystal laser-fusion analysis of MP-32 biotite. Each fusion step analysis consisted of 5–10 crystals of biotite.

zircons into younger pulses of magma (Miller et al., 2007). Studies of similar systems (i.e., upper crustal silicic plutons) with similar datasets have also preferred this interpretation rather than extended crystallization (Miller et al., 2007; Walker et al., 2007; Tappa et al., 2011). Furthermore, many the ‘old’ zircon populations are from analyses of the interior of the zircons, where cores are visible.

The relationship between U/Pb and $^{40}\text{Ar}/^{39}\text{Ar}$ ages also suggests that the zircon age distribution is related to recycling of zircon rather than extended zircon crystallization. After removing UNMIX zircon age populations that are younger than the corresponding biotite ages, the next oldest zircon age population is commonly temporally indistinguishable from or slightly older (i.e., less than several 100 ka) than the biotite age, suggesting rapid cooling from zircon saturation temperature. This is consistent with a shallow depth of emplacement (Toulmin and Hammarstrom, 1990) and high exhumation and erosion rates that characterized central Colorado during the Eocene (Epis and Chapin, 1975). It is highly unexpected that magmas in the shallow crust would remain above the solidus for several Ma crystallizing zircon and therefore not cool rapidly, only to cool rapidly once zircon crystallization was complete.

Finally, the presence of Proterozoic zircon cores in many samples, especially the Mt. Princeton and Mt. Aetna units, sheds light on the crystallization history of the Mt. Aetna caldera complex. Preserved xenocrystic Proterozoic zircons indicate that magmas were zircon saturated during emplacement. If magmas were zircon undersaturated, xenocrystic zircon would have rapidly dissolved (Miller et al., 2007). Though this observation does not rule out the possibility of an extended zircon crystallization history, it does indicate that the Mt. Princeton and Mt. Aetna magmas were capable of incorporating antecrustic zircon without dissolution. Invoking extended crystallization is not necessary to explain the intra-sample UNMIX age populations.

In light of our justification, our interpretation of the zircon age data is as follows. If the youngest zircon population is the same age (within 2σ) or older than the biotite or sanidine age, that population is interpreted as the timing of zircon crystallization and the best estimate for age of magma emplacement (e.g., Fig. 2e). If the youngest UNMIX age is younger than the corresponding biotite age, the next oldest age population is interpreted as the best age of zircon crystallization and pluton emplacement (e.g., Fig. 2f), as long as these ages were geologically consistent with field relationships. For samples that contained additional, older populations that commonly correlate to the interiors or cores of zircons, these ‘old’ populations are interpreted as antecrusts.

6.2. Magmatic history of the Mt. Aetna caldera complex

U/Pb and $^{40}\text{Ar}/^{39}\text{Ar}$ geo- and thermochronology of volcanic and plutonic rocks from the Mt. Aetna caldera complex record the emplacement, eruption, preservation, and thermal history of caldera-related silicic magmas. Fig. 9 summarizes the Mt. Aetna geochronology and thermochronology. U/Pb and $^{40}\text{Ar}/^{39}\text{Ar}$ geochronology indicate protracted magmatism between 38.8 and 30.8 Ma. The Wall Mountain Tuff erupted at 37.3 Ma. Currently exposed parts of the Mt. Princeton batholith were emplaced between 35.9 and 35.2 Ma. The batholith is interpreted to represent both post-Wall Mountain Tuff and pre-Badger Creek Tuff magmatism. The source caldera for the 37.3 Wall Mountain Tuff is interpreted to have been in the same geographic location as the Mt. Princeton batholith, but all physical evidence for the caldera (e.g., intracaldera tuff, ring faults, postcaldera lavas) has been eroded. The Badger Creek Tuff erupted at 34.3 Ma from the Mt. Aetna caldera. Based on the chemical and temporal similarity, the ring dike and Mt. Aetna quartz monzonite are interpreted to be the intrusive geochemical equivalent of Badger Creek Tuff (i.e., nonerupted tuff). The youngest intrusions were emplaced at ~31 Ma and are the most evolved melts. The youngest intrusions caused widespread reheating and thermal resetting of biotite and K-feldspar in many of the older intrusions.

6.2.1. The Wall Mountain Tuff-Mt. Princeton batholith connection

The crystal-rich, low-SiO₂, rhyolitic, Wall Mountain Tuff erupted at 37.25 ± 0.08 Ma (Fig. 3). The timing of Wall Mountain Tuff zircon crystallization, 37.66 ± 0.35 Ma (Fig. 2a), is slightly older, but statistically indistinguishable to the sanidine age. Based on the location of outcrops within paleovalleys and up to 140 km to the east of the Mt. Princeton batholith, the outflow covered a minimum area of 10,400 km² (Epis and Chapin, 1975; Shannon, 1988). The total volume of the Wall Mountain Tuff is estimated to be ~1000 km³ (Lipman, 2007). Because the Wall Mountain Tuff was deposited directly onto the late Eocene erosional surface (Epis and Chapin, 1975), the eruption age of the tuff provides a minimum estimate for the age of this erosional horizon.

The Mt. Princeton batholith was rapidly emplaced into the upper crust. U/Pb zircon crystallization ages of the Mt. Princeton batholith are between 35.85 ± 0.48 and 35.15 ± 0.46 Ma. Using the published geochemistry (Shannon et al., 1987; Shannon, 1988; Toulmin and Hammarstrom, 1990), calculated zircon saturation temperatures for the Mt. Princeton batholith range from 770 to 780 °C. The zircon saturation temperature of the Mt. Princeton quartz monzonite is close to the solidus temperature for rocks of similar composition and emplacement

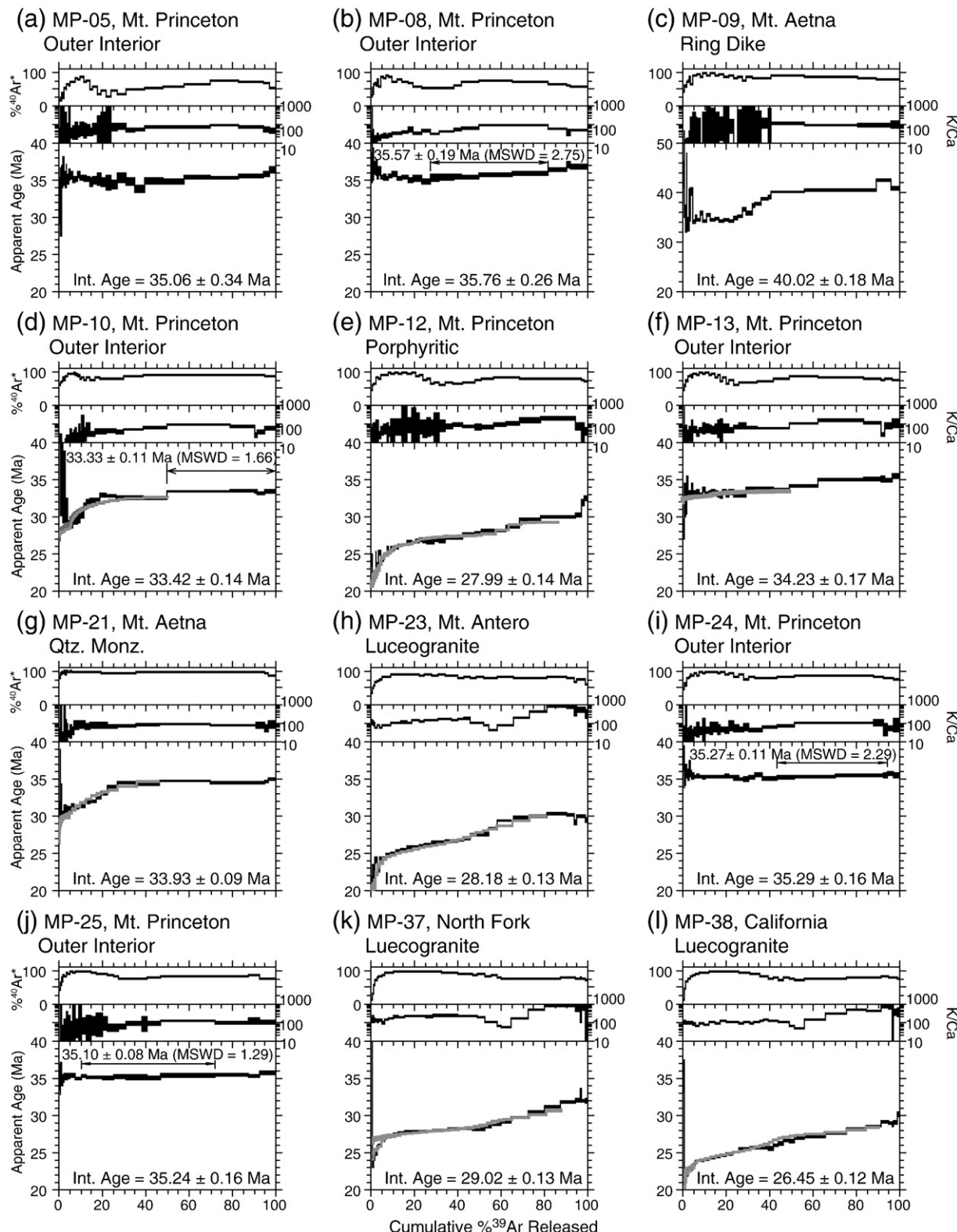


Fig. 6. Age spectra for the plutonic K-feldspar analyses. Auxiliary plots include K/Ca and radiogenic yield (%⁴⁰Ar*). All errors are reported at 2 σ . The gray age spectra represent the modeled age spectra that were used to generate the MDD thermal histories.

depth (Miller et al., 2003; Michel et al., 2008; Tappa et al., 2011). Therefore, the zircon crystallization ages of the Mt. Princeton batholith are interpreted to accurately represent the timing of magma emplacement. Discrete magmatic events, the assembly pattern, and intrusive filling rates of the Mt. Princeton batholith could not be determined because of the relatively large uncertainty associated with LA-ICP-MS ages and

the apparently rapid emplacement rate. However, our results agree with CA-TIMS analyses (35.82 ± 0.10 to 35.37 ± 0.09 Ma; Mills, 2012), which suggest the Mt. Princeton batholith was emplaced rapidly within a 1 Ma period or less. The high-precision CA-TIMS analyses also indicate the batholith was incrementally assembled (Mills, 2012), similar to other silicic systems (Tuolumne Intrusive Suite - Coleman et al., 2004;

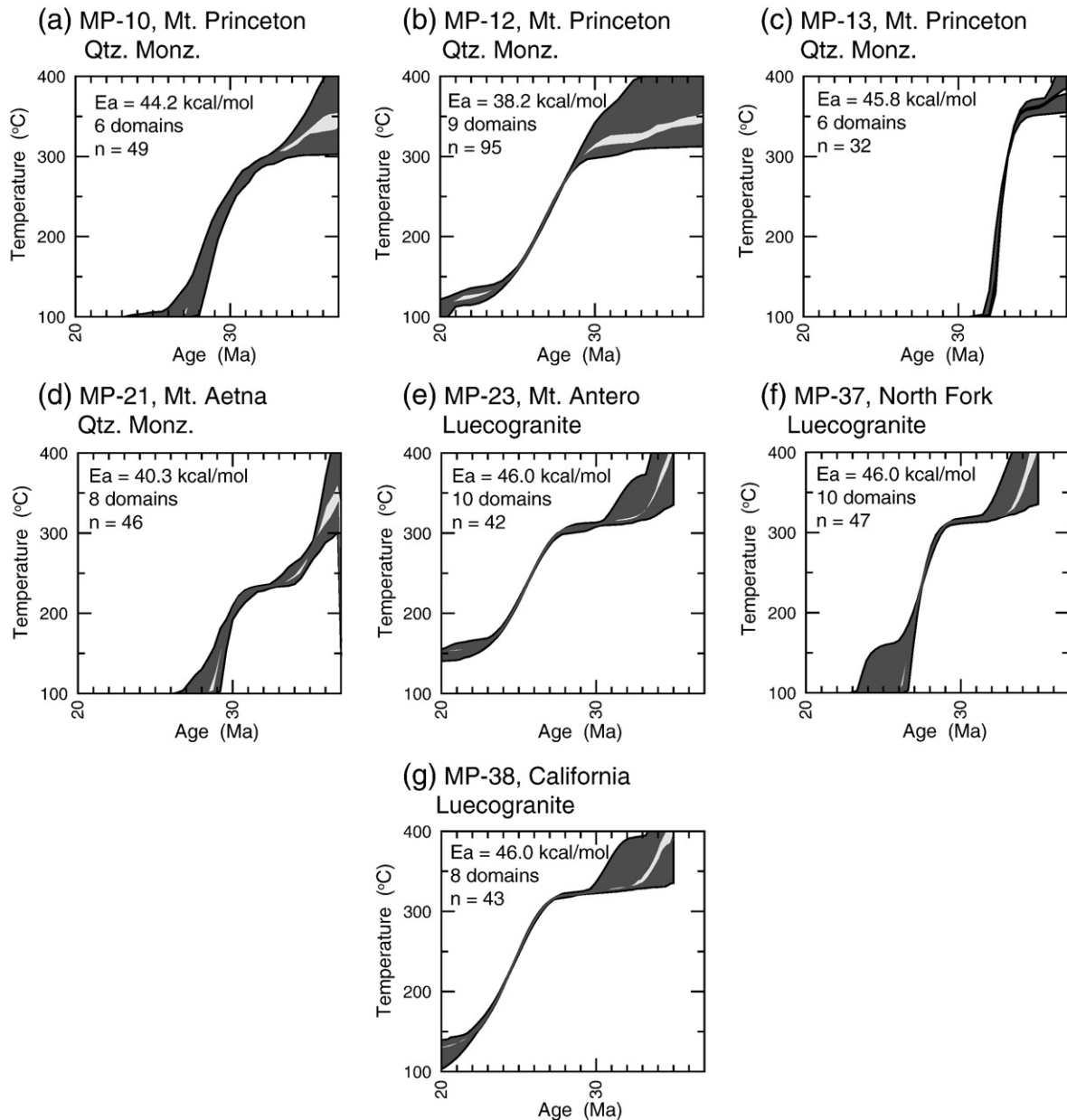


Fig. 7. Monotonic MDD cooling histories generated for the plutonic K-feldspar. The dark gray band is the 90% confidence interval of the entire distribution, whereas the light gray band is the 90% confidence interval of the mean. Activation energy, number of domains, and number of solutions are also provided.

Mt. Stuart batholith and Tenpeak intrusion - Matzel et al., 2006; Spirit Mountain batholith - Walker et al., 2007; Torres del Paine laccolith - Michel et al., 2008; Latir volcanic field - Tappa et al., 2011 and Zimmerer and McIntosh, 2012). This interpretation is consistent with geologic mapping, which has shown that the Mt. Princeton batholith is composed of numerous, near-horizontal compositional and textural horizons (Shannon, 1988).

Though previous studies proposed that the Mt. Princeton batholith was the source for the Wall Mountain Tuff, new U/Pb and $^{40}\text{Ar}/^{39}\text{Ar}$ ages of the Mt. Princeton batholith indicate that the batholith is too young to be the crystallized source magma chamber. Shannon (1988) suggested that the clinopyroxene-bearing border units (MP-03 in this study) might represent part of the nonerupted Wall Mountain Tuff. However, this unit yielded a zircon crystallization age of 35.21 ± 0.51 Ma. The corresponding $^{40}\text{Ar}/^{39}\text{Ar}$ biotite age (35.78 ± 0.11 Ma) is analytically indistinguishable at the 2σ confidence level, but suggests that the emplacement age of this unit might be closer to 35.7 Ma. Regardless, our results from this sample,

as well as all the Mt. Princeton intrusive samples, suggest zircon crystallization and magma emplacement ~ 1 and 2 Ma after the eruption of the Wall Mountain Tuff. This conclusion supports the previous geochemical investigation (Campbell, 1994), which, based on the differences in REE, trace elements, and radiogenic Sr-isotopes, suggested that the Mt. Princeton batholith and Wall Mountain Tuff were not cogenetic. We suspect that the emplacement of the Mt. Princeton batholith into the relatively shallow crust caused some smaller-volume eruptions that commonly characterize pre- and postcaldera volcanism, but these features are now eroded. The available geochronology of the Southern Rocky Mountain volcanic field (McIntosh and Chapin, 2004) does not indicate any large-volume ignimbrite eruptions during the emplacement of the Mt. Princeton batholith.

6.2.2. The Badger Creek Tuff and Mt. Aetna caldera intrusion: volcanic-plutonic pairs

Following the emplacement and exhumation of the Mt. Princeton batholith, the Badger Creek Tuff erupted at 34.26 ± 0.06 Ma (Fig. 3).

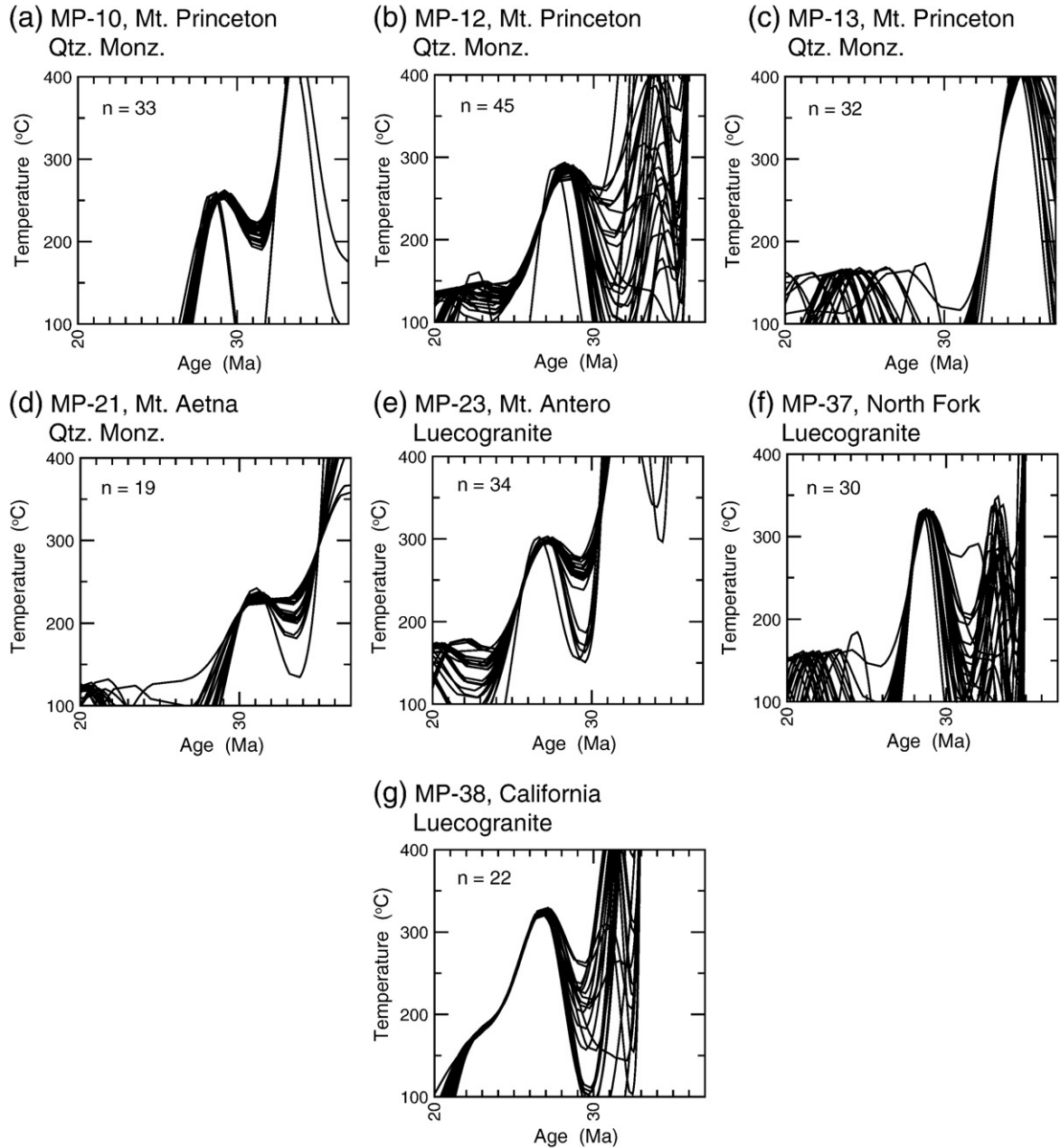


Fig. 8. Unconstrained MDD thermal histories generated for the plutonic K-feldspar. Each thermal history corresponds to a unique solution to the diffusion parameters. Activation energy and number of domains are the same as those reported in Fig. 7.

During the eruption of the Badger Creek Tuff, the Mt. Aetna caldera collapsed in a trap-door style (Shannon, 1988). The greatest subsidence occurred in the southern portion of the caldera (Shannon et al., 1987; Toulmin and Hammarstrom, 1990). Numerous studies have correlated the intracaldera and outflow Badger Creek Tuff using geochemical, paleomagnetic, and geochronologic techniques (Shannon, 1988; Campbell, 1994; McIntosh and Chapin, 2004). The ages of intracaldera (MP-36) and outflow (MP-30 and -31) Badger Creek Tuff are analytically indistinguishable, which supports the correlation of these previous studies. The geochemistry of numerous intracaldera and outflow Badger Creek Tuff samples are similar, indicating that the dacitic, crystal-rich Badger Creek Tuff is not compositionally zoned (Shannon et al., 1987; Campbell, 1994).

LA-ICP-MS U/Pb zircon ages of the Badger Creek Tuff outflow sheet are statistically older than $^{40}\text{Ar}/^{39}\text{Ar}$ sanidine ages. LA-ICP-MS zircon analyses yielded an U/Pb age of 34.83 ± 0.22 Ma. Mills (2012) reported a slightly younger and more precise CA-TIMS age of 34.47 ± 0.05 Ma.

The discrepancy between U/Pb and $^{40}\text{Ar}/^{39}\text{Ar}$ ages of the Badger Creek Tuff may indicate 570 ± 280 ka of pre-eruption zircon residence in Badger Creek Tuff magma chamber. Alternatively, the older U/Pb age may be related to an inaccurate intercalibration of the U/Pb and K/Ar systems (Bachmann et al., 2007b; Kuiper et al., 2008; Renne et al., 2010).

During or shortly after caldera collapse, magma that is compositionally similar to the Badger Creek Tuff intruded into the ring faults, caldera vents, and intracaldera deposits. LA-ICP-MS U/Pb zircon ages of the ring dike and Mt. Aetna quartz monzonite are 34.68 ± 0.26 Ma and 34.26 ± 0.59 . Mills (2012) reported a more precise, yet older CA-TIMS U/Pb zircon age of 34.95 ± 0.04 Ma for the Mt. Aetna quartz monzonite intrusion. The compositional similarity of the two intrusions and the analytically indistinguishable U/Pb ages suggest that the Mt. Aetna ring dike and quartz monzonite pluton are exposed portions of the same intrusion.

U/Pb and $^{40}\text{Ar}/^{39}\text{Ar}$ ages suggest that the Badger Creek Tuff magma chamber was incrementally assembled during a ~500 ka period prior

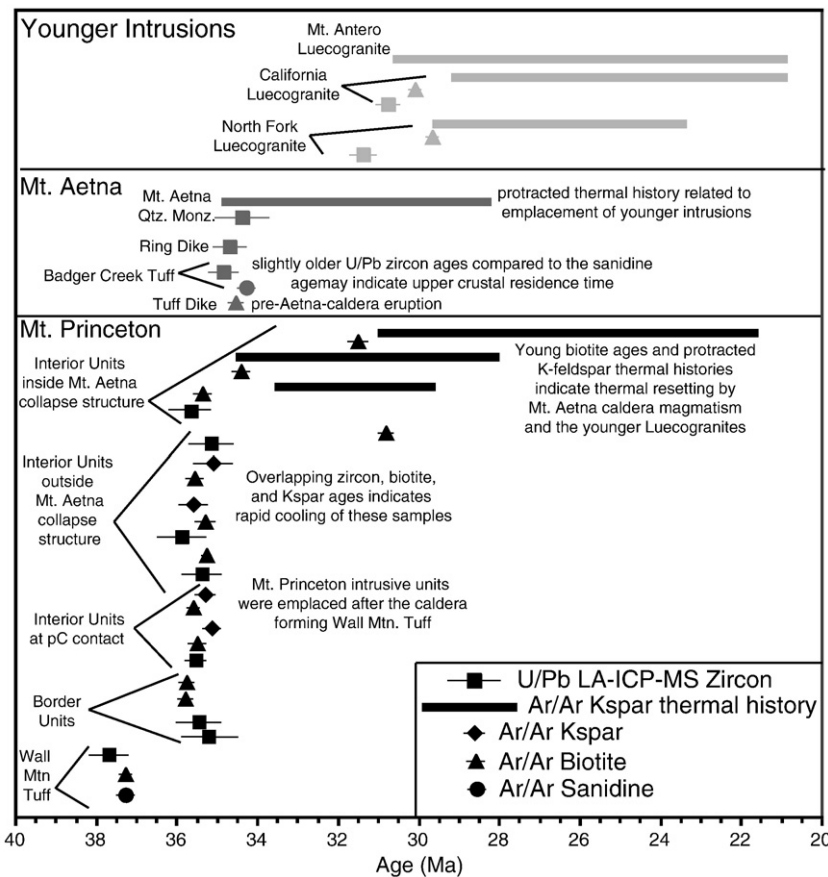


Fig. 9. Summary of the geochronology and thermochronology of the Mt. Aetna caldera complex. All errors are reported at 2 σ . U/Pb zircon ages correspond to the bold ages in Table 1. Antecrustic zircon populations are not represented on this plot. Bold horizontal lines represent the range of ages observed in K-feldspar age spectra and do not imply slow cooling.

to the Mt. Aetna caldera collapse. The compositional similarity of the ring dike, Mt. Aetna quartz monzonite, and Badger Creek Tuff suggests that the units are genetically related (Shannon et al., 1987; Campbell, 1994). Caldera-related intrusions that are compositionally identical to the caldera-forming ignimbrite are commonly interpreted to be the nonerupted geochemical equivalent of the ignimbrite (Lipman et al., 1986; Seager and McCurry, 1988; Johnson et al., 1989; Lipman, 2007; John et al., 2008). If the discrepancy between U/Pb and $^{40}\text{Ar}/^{39}\text{Ar}$ ages is attributed solely to pre-eruptive zircon growth, this implies that magma similar in composition to the Badger Creek Tuff was accumulating in the upper crust prior to the caldera formation. The Mt. Aetna quartz monzonite yielded zircon crystallization ages identical to the eruption age, albeit the LA-ICP-MS age has a large uncertainty. The ring dike yielded a slightly older age of 34.7 Ma. Zircons in the Badger Creek Tuff are the oldest. This range of zircon crystallization ages suggests that the Badger Creek Tuff magma chamber was assembled during a ~500 ka period prior to eruption.

The abundant K-feldspar megacrysts in the coarsely porphyritic quartz monzonite are additional evidence for an incremental assembly history of the Badger Creek magma chamber. The texture of the Mt. Aetna quartz monzonite is unlike many intracaldera plutons, which are typically fine-grained to only slightly porphyritic (Fridrich and Mahood, 1984; Lipman et al., 1986; John et al., 2008). Johnson and Glazner (2010) hypothesized that some K-feldspar megacrysts grow via textural coarsening during thermal cycling of incrementally emplaced granitic plutons. The Badger Creek Tuff magma chamber likely experienced numerous thermal cycles during its assembly. During thermal cycling, regions of the magma chamber are envisioned to have texturally evolved into a porphyritic quartz monzonite. K-feldspar in the eruptible portion of the Badger Creek magma chamber exploded during the

eruption, whereas the nonerupted portion of the magma chamber preserved the pre-caldera-collapse texture.

Evidence for prolonged assembly of upper crustal silicic magma chambers has been observed at other caldera systems. The Fish Canyon Tuff, which is lithologically very similar to the Badger Creek Tuff (i.e., crystal-rich, nonzoned, and dacitic), contains zircons that are ~600 ka older than the eruption age (Bachmann et al., 2007b). U/Pb SHRIMP dating of zircons from the compositionally zoned Whakamaru ignimbrite group erupted from the Taupo volcanic center have rims and cores that differ in age by as much as 250 ka, indicating prolonged upper crustal residence (Brown and Fletcher, 1999). Using a world-wide collection of young volcanic rocks, Simon et al. (2008) determined a mean residence time of 200 ka for silicic magmas. This study also determined that larger, explosive eruptions typically had shorter residence times, perhaps due to higher magmatic fluxes needed to drive the eruptions. However, our results indicate that some large volume caldera-forming magma chambers have extended assembly histories.

The Badger Creek eruption was preceded by numerous, small volume eruptions. The Calico Mountain volcanic units consist of intermediate to silicic lavas, tuffs, and breccias. Because of pervasive alteration no attempt was made to date these rocks using the $^{40}\text{Ar}/^{39}\text{Ar}$ method. The only dated pre-Badger Creek volcanic rock is an intrusive tuff dike (MP-32) located in the northwest region of the complex (Fig. 1). The age of this unit is 34.53 ± 0.12 Ma (Fig. 5b). The intrusive tuff dike was originally interpreted as a vent for the Badger Creek Tuff because of similarities in location, mineralogy, and whole-rock geochemistry. The new age of the tuff dike precludes it being a vent for the caldera-forming eruption and instead suggests that the tuff dike represents a small-volume, pre-caldera-collapse eruption. A possible source for this

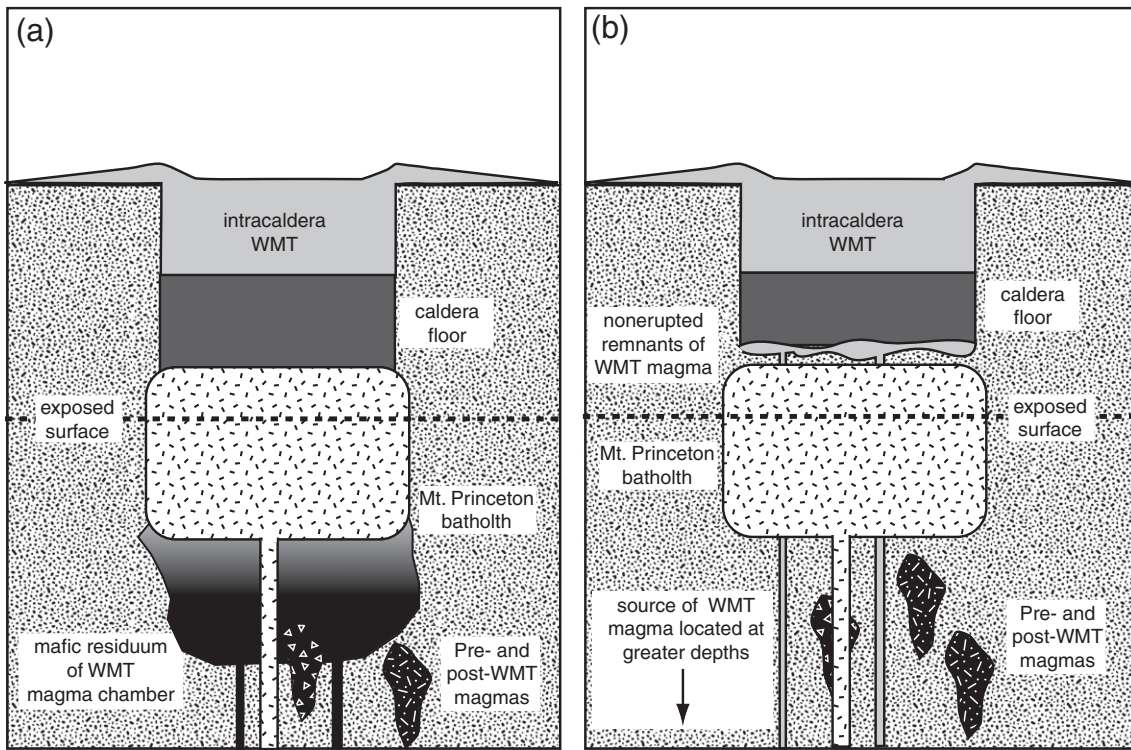


Fig. 10. Schematic diagram illustrating possible models that explain the origin of the 37.3 Ma Wall Mountain Tuff (WMT) in the framework of recently determined U/Pb and $^{40}\text{Ar}/^{39}\text{Ar}$ ages for the Mt. Princeton batholith. Cross-section (not to scale) shows the caldera complex during or shortly after the emplacement of the Mt. Princeton batholith (35.9 to 35.2 Ma). Dashed horizontal line marks the exposed surface prior to the eruption of the Badger Creek Tuff. (a) In this model, the Wall Mountain Tuff was generated via upper crustal in situ fractionation. The caldera-forming eruption drained only the upper silicic parts of the magma chambering, leaving the subjacent, less-fractionated mafic residuum in the caldera-forming magma chamber. The Mt. Princeton batholith was emplaced above the crystal mush in the Wall Mountain Tuff magma chamber. (b) In this model, the Wall Mountain Tuff was generated at deeper (mid- to lower) crustal levels. Only the silicic magmas were emplaced into the upper crust, where they erupted during caldera collapse. The magma chamber efficiently drained, leaving behind small volumes of compositionally identical magma. The Mt. Princeton batholith was emplaced beneath the nonerupted remnants of the caldera-forming magma chamber, which were later obliterated by erosion.

eruption was the Badger Creek Tuff magma chamber, which was incrementally assembling at that time.

6.2.3. Young Luecogranites

The youngest, exposed magmatic events in the Mt. Aetna caldera complex were the emplacement of numerous luecogranites. All exposures of the luecogranites are located in the southeastern portion of the caldera complex. U/Pb zircon ages of the North Fork and California intrusions are 31.37 ± 0.18 and 30.75 ± 0.15 Ma, respectively. Zircon, biotite, and muscovite in the Mt. Antero pluton, the largest exposed luecogranite, were not dated as part of this study. McIntosh and Chapin (2004) reported a weighted mean age of 29.6 Ma for the biotite and muscovite. The oldest steps in the K-feldspar age spectrum (Fig. 6h) yielded ages between 29 and 30 Ma, consistent with the results of McIntosh and Chapin (2004). Consequently, we interpret the timing of Mt. Antero pluton emplacement to be similar to the North Fork and California intrusions.

6.3. Xenocrysts and Antecrysts: Assessing the role of open system magmatic processes

Both volcanic and plutonic samples from the Mt. Aetna caldera complex contain Proterozoic xenocrystic and/or antecrustic zircon. Xenocrystic and antecrustic zircon provide useful information for understanding upper crustal magmatic processes, as well as identifying magmatic events that are not preserved in the exposed intrusions.

6.3.1. Xenocrysts

Ages of xenocrystic zircon and the radiogenic signature of Wall Mountain Tuff indicate that assimilation and/or partial melting of Proterozoic crust were important processes in the genesis of this

rhyolitic magma. LA-ICP-MS U/Pb zircon dating identified numerous 1.4 Ga xenocrystic zircons. However, none of the seven zircons that yielded Proterozoic ages also contained measurable mid-Tertiary rims. This may be because 1) the mid-Tertiary rims, if present, are extremely thin compared to the size of the overall zircon crystals indicating that they were assimilated into the Wall Mountain Tuff magma chamber shortly before the eruption or 2) the Proterozoic zircons were incorporated into the tuff during flow in paleovalleys rather than during storage in the upper crustal caldera-forming magma chamber. Regardless, the initial $^{87}\text{Sr}/^{86}\text{Sr}$ value of the tuff is 0.7094 and the ϵ_{Nd} value is -10.6 (Mills, 2012), indicating that some crustal material was assimilated during genesis of this magma.

Similar to the Wall Mountain Tuff, preserved inherited Proterozoic zircon in the Mt. Princeton batholith indicate open system magmatism during the generation, emplacement and evolution of this intrusion. Three out of eight Mt. Princeton intrusive samples contained zircon with Proterozoic (1.4 – 1.7 Ga) cores and younger rims. Mt Princeton border unit MP-33 contained a single zircon that yielded an age of 477 Ma, which might represent a mixing age between Proterozoic core and mid-Tertiary rim. Exposed country rocks include foliated and nonfoliated 1.4 and 1.7 Ga granitic rocks (Tweto, 1979; Shannon, 1988;) and are the likely source for the inherited zircon. Initial $^{87}\text{Sr}/^{86}\text{Sr}$ ratios of the Mt. Princeton batholith are ~ 0.7075 (Campbell, 1994), which also indicate that crustal material was assimilated into the Mt. Princeton magmas. However, samples that contain Proterozoic xenocrystic zircon are mostly limited to those at or near the contact with country rocks. The extent of in situ upper crustal assimilation and its role in the genetic evolution of the Mt. Princeton batholith may have been limited. This is supported by field observations. Only a few, small (<20 cm) xenoliths were observed at the western contact with country rocks. No xenoliths were observed within the interior of the Mt. Princeton batholith.

Proterozoic xenocrystic zircons were identified in the Badger Creek Tuff and Mt. Aetna ring dike. Rims were not analyzed from zircons that yield Proterozoic ages. $^{87}\text{Sr}/^{86}\text{Sr}$ ratios of the Badger Creek Tuff, Mt. Aetna ring dike, and Mt. Aetna quartz monzonite are ~ 0.7080 (Campbell, 1994), similar to the Mt. Princeton batholith, indicating a crustal component in these magmas.

6.3.2. Antecrysts

With the exception of the Wall Mountain Tuff and North Fork luecogranite, all samples contain antecrustic zircon populations. The age range of antecrustic zircons spans most of the magmatic history of the caldera complex, indicating that material from earlier pulses of magmatism was commonly incorporated into younger magmas.

Antecrustic zircon in the Mt. Princeton intrusive units suggest pre-Wall-Mountain-Tuff magmatism began as early at 38.80 ± 0.39 Ma. Mt. Princeton samples MP-33, -25, -8, -6 (Fig. 2b, e, g, and i, respectively) contain antecrysts that yielded ages older than the 37.3 Ma eruption of the Wall Mountain Tuff. Ages of pre-Wall Mountain Tuff zircon populations range from 38.48 ± 0.57 to 39.19 ± 1.40 Ma. The two oldest populations are very imprecise and therefore do not provide reliable information about the earliest magmatism at the Mt. Aetna caldera complex. The ~ 1.5 Ma period of magmatism prior to the eruption of the Wall Mountain Tuff is consistent with the geochronology of similar caldera systems, which suggests prolong (several 100 ka to several Ma) magmatism commonly occurs prior to caldera collapse (Jellinek and DePaolo, 2003; du Bray et al., 2004; Hildreth, 2004; Lipman, 2007; Zimmerer and McIntosh, 2012).

Three samples contain antecrustic zircon populations that are temporally indistinguishable to the 37.3 Ma eruption of the Wall Mountain Tuff. Mt. Princeton border unit MP-33 (Fig. 2b), Mt. Princeton interior quartz monzonite MP-06 (Fig. 2i), and Mt. Aetna quartz monzonite MP-21 (Fig. 2l) yielded antecrustic zircon ages of 36.93 ± 0.41 , 36.74 ± 0.61 , and 37.17 ± 0.18 Ma, respectively. Considering the relatively large uncertainties associated with these ages, the antecrustic zircon may represent pre-, syn-, or postcaldera magmas. Unless antecrysts were added to the Mt. Princeton batholith via stoping, these zircons suggest pre-Mt. Princeton batholith rocks are located beneath the currently exposed surface (Fig. 10). The implications of these antecrustic zircon populations are fully explored in the last section of the discussion.

Antecrustic zircon in Mt. Princeton batholith, the Mt. Aetna caldera-related rocks, and young luecogranites indicate prolonged open system magmatism during the history of the Mt. Aetna caldera complex. Several Mt. Princeton intrusive samples contain post-Wall-Mountain-Tuff-antecrustic zircon. Populations range in age from 36.27 ± 0.24 (MP-07; Fig. 2d) to 36.48 ± 0.26 Ma (MP-03; Fig. 2c) and are interpreted to represent postcaldera intrusions located at deeper crustal levels. Antecrustic zircons in the Mt. Aetna units (Badger Creek Tuff, ring dike, and quartz monzonite) are temporally indistinguishable to the previously mentioned, nonexposed postcaldera intrusions and range of Mt. Princeton emplacement ages. This is not surprising considering the Mt. Aetna caldera is nested within the Mt. Princeton batholith. Mt. Princeton zircon in the Badger Creek magmas also indicates that upper crustal assimilation was significant. Recall that Mills (2012) reported a CA-TIMS U/Pb zircon age of 34.95 ± 0.04 Ma for the Mt. Aetna quartz monzonite, which is ~ 700 ka older than the eruption age. The CA-TIMS age may represent the initial assembly of the Badger Creek magma chamber. Alternatively, this analysis could be skewed to an older age by an antecrustic zircon core. Finally, 33.59 ± 0.52 Ma antecrustic zircon in the California luecogranite records post-Mt. Aetna caldera magmatism.

6.4. Thermal history of Mt. Aetna caldera complex

6.4.1. The Mt. Princeton thermal history

$^{40}\text{Ar}/^{39}\text{Ar}$ dating indicates that the thermal history of the Mt. Princeton batholith was influenced by the emplacement history and

the proximity to country rocks and younger intrusions. Biotite separates from the outer, border units (MP-02, -03) are the oldest, consistent with cooling near the upper contact with country rocks. Furthermore, CA-TIMS dating by Mills (2012) indicates that the border units are the oldest, and thus may have cooled first. In general, biotite, K-feldspar, and zircon ages from Mt. Princeton interior units located outside the Mt. Aetna collapse structure display a narrow age range from 35.9 to 34.2 Ma. Zircon, biotite, and K-feldspar ages of many samples are statistically indistinguishable indicating rapid cooling following emplacement. This is consistent with shallow emplacement depths and rapid exhumation rates. Contrastingly, Mt. Princeton intrusive units within the Mt. Aetna collapse structure and adjacent to younger intrusions display a prolonged thermal history. For example, sample MP-22 is located < 500 m from the 30.8 Ma California Intrusion. Biotite from MP-22 yielded an age 30.80 ± 0.12 Ma, indistinguishable to the 30.8 Ma zircon emplacement age of the adjacent California intrusion. MDD unconstrained thermal models of sample MP-10 and 12 (Fig. 8a and b, respectively) indicate reheating events at ~ 30 Ma, which also corresponds to emplacement and cooling of the younger luecogranites. MDD models of MP-12 K-feldspar (Fig. 8b) also show evidence for reheating events as young as ~ 22 Ma. Although there are no exposures of ~ 22 Ma igneous rocks in the immediate vicinity of sample MP-12 (McIntosh and Chapin, 2004), a small volume rhyolitic dome, the 22 Ma Raspberry Gulch rhyolite (Campbell, 1994), is located ~ 10 km away along the eastern margin of the complex. This may indicate additional intrusions of this age that are currently not exposed. $^{40}\text{Ar}/^{39}\text{Ar}$ thermochronology of the western and northern outcrops of the Mt. Princeton batholith do not display evidence for reheating events between 30 and 31 Ma, suggesting that luecogranite magmatism was limited to the immediate vicinity of the mapped outcrops.

One sample that did not yield indistinguishable biotite and K-feldspar ages is MP-10 (Fig. 6d), a Mt. Princeton interior unit. Biotite from this sample yielded an integrated age of 35.33 ± 0.16 Ma, indicating cooling to ~ 300 – 350 °C soon after emplacement. The oldest ages observed in the MP-10 K-feldspar age spectrum are from the highest temperature steps, which yielded a plateau age of 33.33 ± 0.11 Ma. MDD unconstrained thermal histories of MP-10 K-feldspar indicate a ~ 400 °C reheating event at 33.3 Ma (Fig. 8a). However, a ~ 400 °C reheating event at 33.3 Ma should have thermally reset the biotite crystals as well. The ~ 2 Ma age discrepancy between the biotite age and ages of K-feldspar high-temperature steps could be related to extremely slow cooling from ~ 350 °C (biotite closure temperature) to 300 °C (closure temperature of the largest K-feldspar domains) between 35.3 and 33.3 Ma. However, this latter scenario seems unlikely considering the shallow depth of emplacement, rapid erosion and exhumation rates, and that most Mt. Princeton samples indicate rapid cooling. The steps that define the K-feldspar plateau were generated during high-temperature analyses. The high-temperature steps correlated to degassing of the largest domains, which are commonly contaminated with excess ^{40}Ar (Foster et al., 1990; Zimmerer and McIntosh, 2012). The anomalous K-feldspar plateau age is interpreted to be related to excess argon and therefore, is not geologically significant. The youngest ages observed in the K-feldspar age spectrum are ~ 29 to 30 Ma, which likely correlate to reheating during emplacement and cooling of the young luecogranites.

6.4.2. Thermal history of the Mt. Aetna caldera-related intrusions

The thermal history of the Mt. Aetna quartz monzonite, like that of the Mt. Princeton batholith, was influenced by proximity to the younger intrusions. The age spectrum of the quartz monzonite K-feldspar is characterized by monotonically increasing steps from 30 to 34 Ma (Fig. 6g). The unconstrained MDD models indicate a reheating event that reaches a maximum temperature of ~ 250 °C at ~ 31 Ma (Fig. 8d), consistent with reheating by younger, adjacent intrusions. K-feldspar from the ring dike yielded a disturbed plateau (Fig. 6c). Accordingly, the age spectrum was not modeled using the MDD theory.

6.4.3. Thermal history of the young luecogranites

$^{40}\text{Ar}/^{39}\text{Ar}$ thermochronology of the luecogranites indicate rapid cooling from magmatic temperatures followed by a protracted thermal history at low temperatures. Biotite ages of the California and North Fork and intrusion are 30.07 ± 0.08 and 29.65 ± 0.09 Ma, respectively. K-feldspar age spectra from the luecogranites samples indicate a protracted thermal history (Fig. 6h, k, and l). For all three samples, the oldest ages in the spectrum are approximately the same age as the timing of emplacement. However, the youngest ages in the age spectra are between 20 and 24 Ma. Because of the shallow depth of emplacement, several Ma of slow cooling through the K-feldspar closure temperature is not likely. MDD unconstrained models of the three samples (Fig. 8e, f, and g) indicate a major reheating event between 27 and 29 Ma and numerous, low-temperature reheating events as young as ~20 Ma. These reheating events are not correlated to known magmatic events. Thus, the youngest ages observed in the age spectra are related to reheating events during the emplacement of unexposed intrusions or possibly K-feldspar recrystallization (Lovera et al., 2002).

6.5. Origin of the Wall Mountain Tuff and Badger Creek Tuff magmas

Because of the widespread distribution of the Wall Mountain Tuff and its potential genetic link to the Mt. Princeton batholith, determining the temporal relationship between the two has been a reoccurring theme of Southern Rocky Mountain volcanic field studies. New LA-ICP-MS U/Pb zircon and $^{40}\text{Ar}/^{39}\text{Ar}$ ages indicate that the Mt. Princeton batholith was emplaced and cooled rapidly several Ma after the 37.3 Ma caldera-forming Wall Mountain Tuff eruption. We propose that the source caldera for the Wall Mountain Tuff was located in the same geographic area as the Mt. Princeton batholith, but at a structurally higher level. This interpretation explains why paleovalleys that contain outflow Wall Mountain Tuff converge near the Mt. Princeton batholith. The source caldera was likely eroded away shortly after the Wall Mountain Tuff eruption. In this framework, the Mt. Princeton batholith represents both post-Wall Mountain Tuff and pre-Badger Creek Tuff magmatism.

Antecrustic zircon in the Mt. Princeton intrusive units and the Mt. Aetna quartz monzonite indicate that magmatism occurred for several Ma prior to the emplacement of the Mt. Princeton batholith. These antecrustic zircon populations range from 38.8 to 36.3 Ma. We believe the abundance of antecrustic zircon that yielded pre-, syn-, and post Wall Mountain Tuff ages, coupled with published studies that indicate caldera eruptions are preceded and followed by voluminous magmatism (Jellinek and DePaolo, 2003; Lipman, 2007), provides substantial evidence to link the Wall Mountain Tuff to a caldera source in the geographic vicinity of the Mt. Princeton batholith.

Additional evidence that suggests the Wall Mountain Tuff erupted from a source near the Mt. Princeton batholith is related to the relative timing of large volume plutonism in relationship to caldera eruptions. Similar caldera-pluton studies have determined that plutons are typically emplaced during syn- or postcaldera magmatism (Lipman, 1984; Lipman et al., 1986; Seager and McCurry, 1988; Lipman, 2007; Tappa et al., 2011; Zimmerer and McIntosh, 2012). Volumetrically significant precaldera intrusions are rare in most single caldera systems. During precaldera magmatism the crust is cold and overpressure created by magmatism fractures the country rock, which causes dike propagation. Early magma emplacement results in eruptions that may efficiently drain the chamber rather than storing and preserving the magma as plutons. However, after continued magmatism, the effective wall-rock viscosity decreases, which is more likely to promote magma storage rather than eruptions (Jellinek and DePaolo, 2003). If the source caldera for the Wall Mountain Tuff was not in the same geographic location as the Mt. Princeton batholith, then the Mt. Princeton batholith is a rare example of a volumetrically significant precaldera intrusion. However, if the Mt. Princeton batholith is interpreted in the framework of a

multi-cyclic caldera system, than the Mt. Princeton batholith represents both post-Wall Mountain Tuff and pre-Badger Creek Tuff magmatism. Following the Wall Mountain Tuff eruption the crust was warm, which favored magma storage. Extension in the upper crust related to the inception of the Rio Grande rift may have also promoted magma storage (Hanson and Glazner, 1995; Petford et al., 2000; Chapin et al., 2004).

High erosion and exhumation rates characterized central Colorado during the late Eocene/early Oligocene. Paleovalleys in central Colorado were repeatedly filled by outflow of regional ignimbrites. Continued erosion re-incised the valleys, which acted as pathways for pyroclastic deposits during subsequent volcanism (Epis and Chapin, 1975; McIntosh and Chapin, 2004). The Mt. Princeton batholith was emplaced at ~3 km depth (Hammarstrom and Zen, 1986), but was exposed at the surface prior to the 34.3 Ma eruption of the Badger Creek Tuff. Using the oldest U/Pb age of the Mt. Princeton batholith (35.9 Ma), this implies an average uplift rate of 1.9 mm/yr, which is similar to some exhumation rates of the Himalayans (Vance et al., 2003; Theide et al., 2004). The point of quantifying the erosion and exhumation rates that characterized the region is to show that they were sufficiently high enough to have obliterated the Wall Mountain Tuff source caldera. However, erosion and exhumation rates must have slowed following the eruption of the 34.3 Ma Badger Creek Tuff. A ~0.5 km thick deposit of intracaldera Badger Creek Tuff is preserved along the southern margin of the Mt. Aetna caldera. Mapping of faulted, well-exposed calderas indicates that the thickness of intracaldera ignimbrites typically ranges from 3 to 5 km (Lipman et al., 1986; Seager and McCurry, 1988; Lipman, 1997; John et al., 2008). This suggests that 2.5 to 4.5 km of intracaldera Badger Creek Tuff has been removed by erosion. If the calculated average exhumation and erosion rates that existed between the emplacement of the Mt. Princeton batholith and the eruption Badger Creek Tuff continued after formation of the Mt. Aetna caldera, the current surface would have been exposed in $1.8 - 3.2 \times 10^6$ yrs. The preservation of some intracaldera Badger Creek Tuff indicates exhumation and erosion rates must have slowed shortly after the Mt. Aetna caldera collapse.

The volume and composition of the nonerupted material in the Wall Mountain Tuff magma chamber is difficult to constrain because it is not preserved as an exposed intrusion. Fig. 10 depicts two possible models for the origin of the Wall Mountain Tuff silicic magmas. Fractionation models predict a 3 to 10:1 intrusive:extrusive ratio (White et al., 2006). For the Wall Mountain Tuff, this corresponds to 3,000 to 10,000 km³ of nonerupted material. Evidence for a 37.3 Ma intrusion of this size is not preserved in the Sawatch Range, nor could that intrusion have been obliterated by the previously described exhumation and erosion. If the Wall Mountain Tuff was generated via crystal-liquid fractionation, this must have occurred below the currently exposed crustal levels and the Mt. Princeton batholith was emplaced above the nonerupted components of the magma chamber (Fig. 10a). Alternatively, several studies have proposed that silicic melts are generated at deep crustal levels and emplaced into the upper crust (Eichelberger et al., 2000; Glazner et al., 2004; Annen et al., 2006). During caldera collapse, the magma chamber may nearly completely drain leaving behind only small-volume intrusions that are compositionally similar to the caldera forming ignimbrite (Roche and Druitt, 2001; Glazner et al., 2004; Tappa et al., 2011; Zimmerer and McIntosh). If this latter model (Fig. 10b) is correct, the calculated exhumation and erosion rates could have been sufficient to erode the nonerupted remnants of the Wall Mountain Tuff magma chamber. Additionally, this could explain the paucity of Wall Mountain Tuff antecrustic zircon populations in the analyzed samples despite comprehensive sampling of the caldera complex. Because of erosion and the limited exposure, both interpretations are highly speculative. This work cannot constrain the exact location of Wall Mountain Tuff genesis within the crust, other than to limit genesis at deeper levels. However, it is consistent with several studies that have suggested silicic magma can be generated in the

mid- to lower crust (Glazner et al., 2004; Dufek and Bergantz, 2005; Annen et al., 2006; Quick et al., 2009; Tappa et al., 2011; Zimmerer and McIntosh, 2012).

Current exposures of the Mt. Aetna caldera provide a limited view of the subcaldera intrusions. The caldera floor, intracaldera ignimbrite, ring structures and dikes, and the structurally highest intrusions of the subcaldera batholith are exposed. Because deeper portions of the Badger Creek Tuff magma chamber are not exposed, we could not fully assess whether the dacitic, Badger Creek Tuff fractionated from a more mafic magma (e.g., andesite) in the upper crust or was generated at deeper crustal levels. In situ crystal fractionation inherently produces zoned magma chambers (Smith, 1979; Hildreth, 2004; Bachmann and Bergantz, 2008). During caldera collapse of zoned magma chambers, the mafic parts of magma chamber are commonly resurgent in the intracaldera sequence or preserved in ring dikes. For example, the exposed resurgent intrusion within the highly-eroded Grizzly Peak caldera, central CO, is reversely zoned (silicic margins with a mafic core). Presumably the compositionally zoned magma chamber was rearranged during resurgence (Fridrich and Mahood, 1984). Evidence for a zoned, upper crustal magma chamber is also preserved at Ossipee caldera. Here, the exposed ring dike contains mingled rhyolite, syenite, and basalt, which were interpreted as residual crystal mush for the caldera-forming ignimbrite (Kennedy and Stix, 2007). Multiple components of the Badger Creek Tuff magma chamber are exposed, including outflow and intracaldera tuff, the tuff dike, and the ring dike that grades into the Mt. Aetna quartz monzonite. The lack of significant compositional zoning in any of these units (Shannon et al., 1987; Campbell, 1994) brings into question the role of in situ crystal fractionation during the genesis of the Badger Creek magmas. Certainly the highly viscous, porphyritic quartz monzonite may have prevented more mafic magma from ascending to higher positions in the magma chamber. Alternatively, upper crustal in situ fractionation may have been a relatively minor or a nearly absent process for generating the dacitic Badger Creek Tuff. Some studies have suggested that dacitic magmas are the dominant composition to reach the upper crust (Bachmann and Bergantz, 2004; Annen et al., 2006; de Silva and Gosnold, 2007). Perhaps with additional residence time in the upper crust, the Badger Creek Tuff may have fractionated and evolved to more silicic compositions.

7. Conclusions

Establishing the spatial, temporal, and chemical relationships of upper crustal plutons and ignimbrites provides important information for understanding caldera-related magmatic processes. U/Pb and $^{40}\text{Ar}/^{39}\text{Ar}$ ages document the emplacement, eruption, and thermal history of the Mt. Aetna caldera complex silicic magmas. The $^{40}\text{Ar}/^{39}\text{Ar}$ ages of volcanic rocks and the U/Pb plutonic zircon ages indicate that magmatism at the Mt. Aetna complex spanned a minimum duration of 8 Ma, from 38.8 to 30.8 Ma. Peak magmatic output occurring during the eruption of two caldera-forming ignimbrites, the 37.3 Ma Wall Mountain Tuff and the 34.3 Ma Badger Creek Tuff. With the exception of the Mt. Aetna quartz monzonite and ring dike, all the exposed intrusions were emplaced during pre- and/or postcaldera caldera magmatism. Antecrustic zircons were found in nearly every sample and the age populations span most of the magmatic history of the caldera complex. Assimilation and recycling of crystalline material from earlier pulses of magmatism were apparently significant processes during the evolution of this nested caldera system. Thermochronology indicates a prolonged thermal history of the subcaldera batholith due to protracted pluton emplacement.

Though the Wall Mountain Tuff and Mt. Princeton batholith have been previously interpreted as a classic example of the volcanic-plutonic rock pair produced by in situ fractionation of a large-volume magma chamber in the upper crust, the batholith is in fact too young to be the source for the tuff. Zircon crystallization ages of the batholith indicate emplacement during post-Wall Mountain Tuff

magmatism. However, antecrustic zircon in the Mt. Princeton batholith range from 38.8 to 36.3 Ma, suggesting the Wall Mountain Tuff erupted from a source near the Mt. Princeton batholith. The absence of a coeval, less-fractionated, residual crystal mush for the Wall Mountain Tuff, despite having some of most well-exposed subcaldera intrusions, indicate that this caldera-forming magma must have been generated below the currently exposed Mt. Princeton batholith. Though in situ fractionation in the upper crust certainly occurs and is a fundamentally important magmatic process, our research suggests that it is not necessarily the only mechanism capable of generating caldera-forming silicic magmas. Silicic magmas can be generated at deeper crustal levels than the shallow magma chambers from which they erupt.

The Mt. Aetna quartz monzonite and ring dike are interpreted to represent nonerupted, geochemically equivalent intrusions to the Badger Creek Tuff. Zircon populations in the tuff, ring dike, and quartz monzonite are as much as 500 ka older than the 34.3 Ma eruption age. This suggests that the Badger Creek Tuff magma chamber was incrementally assembled in the upper crust and was a long-lived feature. Prior to eruption, the caldera-forming magma chamber was compositionally uniform but chronologically heterogeneous. Though the ring dike and Mt. Aetna quartz monzonite are interpreted to have been part of the Badger Creek Tuff magma chamber, the intrusive units are chemically similar to the Badger Creek Tuff and therefore are not interpreted as the complimentary, less-fractionated, residual crystal mush.

Acknowledgements

This research was supported by a NSF grant (EAR-1050188). We would like to thank the support of the New Mexico Tech Graduate Association, the Colorado Scientific Society, the New Mexico Bureau of Geology and Mineral Resources, and the New Mexico Geological Society for funding portions of the fieldwork and analytical costs. George Gehrels and Victor Valencia helped acquire LA-ICP-MS zircon ages. Peter Lipman, Drew Coleman, Ryan Mills, Matt Heizler, Kent Condie, and Andy Campbell provided invaluable feedback during the course of this research and preparation of this manuscript. Finally, we would like to thank de Silva and Antonia Castro for their thoughtful reviews, as well as Joan Marti for his professional guidance during the editing of this manuscript.

Appendix A. Supplementary data

Supplementary data to this article can be found online at <http://dx.doi.org/10.1016/j.jvolgeores.2012.08.007>.

References

- Annen, C., 2009. From plutons to magma chambers: Thermal constraints on the accumulation of eruptible silicic magma in the upper crust. *Earth and Planetary Science Letters* 284, 409–416.
- Annen, C., Blundy, J.D., Sparks, R.S.J., 2006. The genesis of intermediate and silicic magmas in deep crustal hot zones. *Journal of Petrology* 47, 505–539.
- Bachmann, O., Bergantz, G., 2004. On the origin of crystal-poor rhyolites: Extracted from batholith crystal mushes. *Journal of Petrology* 45, 1565–1582.
- Bachmann, O., Bergantz, G.W., 2008. Deciphering magma chamber dynamics from styles of compositional zoning in large silicic ash flow sheets. *Reviews in Mineralogy and Geochemistry* 69, 651–674.
- Bachmann, O., Dungan, M., Lipman, P.W., 2002. The Fish Canyon Magma Body, San Juan volcanic field, Colorado: Rejuvenation and eruption of an upper-crustal batholith. *Journal of Petrology* 43, 1369–1503.
- Bachmann, O., Miller, C.F., de Silva, S.L., 2007a. The volcanic-plutonic connection as a stage for understanding crustal magmatism. *Journal of Volcanology and Geothermal Research* 167, 1–23.
- Bachmann, O., Oberlie, F., Dungan, M.A., Meier, M., Mundil, R., Fischer, H., 2007b. $^{40}\text{Ar}/^{39}\text{Ar}$ and U/Pb dating of the Fish Canyon magmatic system, San Juan volcanic field, Colorado; evidence for an extended crystallization history. *Chemical Geology* 236, 134–166.

- Bacon, C.R., Druitt, T.H., 1988. Compositional evolution of the zoned calc-alkaline magma chamber of Mount Mazama, Crater Lake, Oregon. *Contributions to Mineralogy and Petrology* 98, 224–256.
- Baldridge, W.S., Olsen, K.H., 1989. The Rio Grande rift. *American Scientist* 77, 240–247.
- Brown, S.J.A., Fletcher, I.R., 1999. SHRIMP U-Pb dating of the preeruptive growth history of zircons from the 340 ka Whakamaru Ignimbrite, New Zealand: Evidence for >250 k.y. magma residence times. *Geology* 27, 1035–1038.
- Buddington, A.F., 1959. Granite emplacement with special reference to North America. *Geological Society of America Bulletin* 70, 671–748.
- Campbell, S.K., 1994. A geochemical and strontium isotopic investigation of Laramide and younger igneous rocks in central Colorado, with emphasis on the petrogenesis of the Thirtynine Mile volcanic field. Ph.D. Thesis, Florida State University, Tallahassee, FL, United States (USA).
- Chapin, C.E., Wilks, M., McIntosh, W.C., 2004. Space-time patterns of Late Cretaceous to present magmatism in New Mexico—comparison with Andean volcanism and potential for future volcanism. *New Mexico Bureau of Geology and Mineral Resources Bulletin* 160, 13–40.
- Coleman, D.S., Gray, W., Glazner, A.F., 2004. Rethinking the emplacement and evolution of zoned plutons: Geochronological evidence for incremental assembly of the Tuolumne Intrusive Suite, California. *Geology* 32, 433–436.
- Coney, P.J., Reynolds, S.J., 1977. Cordilleran Benioff zones. *Nature* 270, 403–407.
- Davies, J.H., Stevenson, D.J., 1992. Physical model of source region of subduction zone volcanoes. *Journal of Geophysical Research* 97, 2037–2070.
- de Silva, S.L., Gosnold, W.D., 2007. Episodic construction of batholiths: Insights from the spatiotemporal development of an ignimbrite flare-up. *Journal of Volcanology and Geothermal Research* 167, 320–335.
- Deering, C.D., Bachmann, O., 2010. Trace element indicators of crystal accumulation in silicic igneous rocks. *Earth and Planetary Science Letters* 297, 324–331.
- du Bray, E.A., Snee, L.W., Pallister, J.S., 2004. Geochemistry and geochronology of middle Tertiary volcanic rocks of the central Chiricahua Mountains, Southeast Arizona. U.S. Geological Survey Professional Paper, 1684, 57 pp.
- Dufek, J., Bergantz, G.W., 2005. Lower crustal magma genesis and preservation: a stochastic framework for the evaluation of basalt-crust interactions. *Journal of Petrology* 46, 2167–2195.
- Eichelberger, J.C., Chertkoff, D.G., Dreher, S.T., Nye, C.J., 2000. Magmas in collision: re-thinking chemical zonation in silicic magmas. *Geology* 28, 603–606.
- Epis, R.C., Chapin, C.E., 1975. Geomorphic and tectonic implications of the post-Laramide, late Eocene erosion surface in the Southern Rocky Mountains. *Geological Society of America Memoir*, 144, pp. 45–74.
- Fleck, R.J., Sutter, J.F., Elliot, D.H., 1977. Interpretation of discordant $^{40}\text{Ar}/^{39}\text{Ar}$ age-spectra of Mesozoic tholeiites from Antarctica. *Geochimica et Cosmochimica Acta* 41, 15–32.
- Foster, D.A., Harrison, T.M., Copeland, P., Heizler, M.T., 1990. Effects of excess argon within large diffusion domains on K-feldspar age. *Geochimica et Cosmochimica Acta* 54, 1699–1708.
- Francis, P., Oppenheimer, C., 2004. Volcanoes. Oxford University Press, Oxford.
- Fridrich, C.J., Mahood, G.A., 1984. Reverse zoning in the resurgent intrusions of the Grizzly Peak cauldron, Sawatch Range, Colorado. *Geological Society of America Bulletin* 95, 779–787.
- Fridrich, C.J., DeWitt, E., Bryant, B., Steve, R., Smith, R. P., 1998. Geologic map of the Collegiate Peaks Wilderness Area & the Grizzly Peak caldera, Sawatch Range, central Colorado. U. S. Geological Survey, Miscellaneous Investigations Series map I-2565, scale 1:5000, 29 pp.
- Gehrels, G.E., Valencia, V.A., Ruiz, J., 2008. Enhanced precision, accuracy, efficiency, and spatial resolution of U-Pb ages by laser ablation-multicollector-inductively coupled plasma-mass spectrometry. *Geochemistry, Geophysics, Geosystems* 9 (13pp.).
- Gillespie, A.R., Hunkele, J.C., Wasserburg, G.J., 1982. An assessment of $^{40}\text{Ar}/^{39}\text{Ar}$ dating of incompletely degassed xenoliths. *Journal of Geophysical Research Letters* 87, 9247–9257.
- Glazner, A.F., 1994. Foundering of mafic plutons and density stratification of continental crust. *Geology* 22, 435–438.
- Glazner, A.F., Bartley, J.M., Coleman, D.S., Gray, W.M., Taylor, R.Z., 2004. Are plutons assembled over millions of years by amalgamation from small magma chambers? *Geological Society of America Today* 14, 4–11.
- Glazner, A.F., Coleman, D.S., Bartley, J.M., 2008. The tenuous connection between high-silica rhyolites and granodiorite plutons. *Geology* 36, 183–186.
- Hammarstrom, J.M., Zen, E., 1986. Aluminum in hornblende: An empirical igneous geobarometer. *American Mineralogist* 71, 1297–1313.
- Hanson, R.B., Glazner, A.F., 1995. Thermal requirements for extensional emplacement of granitoids. *Geology* 23, 213–216.
- Harrison, T.M., Heizler, M.T., Lovera, O.M., Wenji, C., Grove, M., 1994. A chlorine disinfectant for excess argon released from K-feldspar during step heating. *Earth and Planetary Science Letters* 123, 95–104.
- Heizler, M.T., Lux, D.R., Decker, E.R., 1988. The age and cooling history of The Chain of Ponds and Big Island plutons and the Spider Lake Granite, west-central Maine and Quebec. *American Journal of Science* 288, 925–952.
- Hildreth, W., 1981. Gradients in silicic magma chambers: Implications for lithospheric magmatism. *Journal of Geophysical Research* 86, 10153–10192.
- Hildreth, W., 2004. Volcanological perspectives on Long Valley, Mammoth Mountain and Mono Craters: several contiguous but discrete systems. *Journal of Volcanology and Geothermal Research* 136, 169–198.
- Hilton, D.R., 1996. The helium and carbon isotope systematics of a continental geothermal system: results from monitoring studies at the Long Valley caldera (California, U.S.A.). *Chemical Geology* 127, 269–295.
- Hodges, K.V., 1991. Pressure-temperature-time paths. *Annual Reviews Earth and Planetary Science Letters* 19, 207–236.
- Jellinek, A.M., DePaolo, D.J., 2003. A model for the origin of large silicic magma chambers: Precursors of caldera-forming eruptions. *Bulletin of Volcanology* 65, 363–381.
- John, D.A., Henry, C.D., Colgan, J.P., 2008. Magmatic and tectonic evolution of the Caetano caldera, north-central Nevada: A tilted, mid-Tertiary eruptive center and source of the Caetano Tuff. *Geosphere* 4, 75–106.
- Johnson, C.M., 1991. Large-scale crustal formation and lithosphere modification beneath middle to late Cenozoic calderas and volcanic fields, western North America. *Journal of Geophysical Research* 96, 13485–13507.
- Johnson, B.R., Glazner, A.F., 2010. Formation of K-feldspar megacrysts in granodioritic plutons by thermal cycling and late-stage textural coarsening. *Contributions to Mineralogy and Petrology* 159, 599–619.
- Johnson, C.M., Lipman, P.W., 1988. Origin of metaluminous and alkaline volcanic rocks of the Latir volcanic field, northern Rio Grande Rift, New Mexico. *Contributions to Mineralogy and Petrology* 100, 107–128.
- Johnson, C.M., Czamanske, G.K., Lipman, P.W., 1989. Geochemistry of intrusive rocks associated with the Latir volcanic field, New Mexico and contrasts between evolution of plutonic and volcanic rocks. *Contributions to Mineralogy and Petrology* 103, 90–109.
- Kennedy, B., Stix, J., 2007. Magmatic processes associated with caldera collapse at Ossipee ring dyke, New Hampshire. *Geological Society of American Bulletin* 119, 3–17.
- Klemm, L.M., Pettke, T., Heinrich, C.A., 2008. Fluid and source magma evolution of the Questa porphyry Mo deposit, New Mexico, USA. *Mineralium Deposita* 43, 533–552.
- Knesel, K.M., Duffield, W.A., 2007. Gradients in silicic eruptions caused by rapid inputs from above and below rather than protracted chamber differentiation. *Journal of Volcanology and Geothermal Research* 167, 181–197.
- Kuiper, K.F., Deino, A., Hilgen, F.J., Krijgsman, W., Renne, P.R., Wijbrans, J.R., 2008. Synchronizing rock clocks of earth history. *Science* 320, 500–504.
- Lawton, T.F., McMillan, N.J., 1999. Arc abandonment as a cause for passive continental rifting: Comparison of the Jurassic Mexican Borderland Rift and the Cenozoic Rio Grande Rift. *Geology* 27, 779–782.
- Lipman, P.W., 1984. The roots of ash flow calderas in western North America: Windows into the tops of granitic batholiths. *Journal of Geophysical Research* 89, 8801–8841.
- Lipman, P.W., 1997. Subsidence of ash-flow calderas: relation to caldera size and magma-chamber geometry. *Bulletin of Volcanology* 59, 198–218.
- Lipman, P.W., 2007. Incremental assembly and prolonged consolidation of Cordilleran magma chambers: evidence from the Southern Rocky Mountain volcanic field. *Geosphere* 3, 42–70.
- Lipman, P.W., McIntosh, W.C., 2008. Eruptive and noneruptive calderas, northeastern San Juan Mountains, Colorado: Where did the ignimbrites come from? *Geological Society of America Bulletin* 120, 771–795.
- Lipman, P.W., Doe, B.R., Hedge, C.E., Steven, T.A., 1978. Petrologic evolution of the San Juan volcanic field, southwestern Colorado: Pb and Sr isotope evidence. *Geological Society of America Bulletin* 89, 59–82.
- Lipman, P.W., Mehnert, H.H., Naeser, C.W., Keller, G.R., 1986. Evolution of the Latir volcanic field, northern New Mexico and its relation to the Rio Grande Rift, as indicated by potassium-argon and fission track dating. *Journal of Geophysical Research* 91, 6329–6345.
- Lo, C., Onstott, T.C., 1989. ^{39}Ar recoil artifacts in chloritized biotite. *Geochimica et Cosmochimica Acta* 53, 2967–2711.
- Lovera, O.M., Richter, F.M., Harrison, T.M., 1989. $^{40}\text{Ar}/^{39}\text{Ar}$ thermochronology for slowly cooled samples having a distribution of domain sizes. *Journal of Geophysical Research* 94, 17917–17935.
- Lovera, O.M., Richter, F.M., Harrison, T.M., 1991. Diffusion domains determined by ^{39}Ar released during step heating. *Journal of Geophysical Research* 96, 2057–2069.
- Lovera, O.M., Grove, M., Harrison, T.M., Mahon, K.I., 1997. Systematic analysis of K-feldspar $^{40}\text{Ar}/^{39}\text{Ar}$ step heating results I: Significance of activation energy determinations. *Geochimica et Cosmochimica Acta* 61, 3171–3192.
- Lovera, O.M., Grove, M., Harrison, T.M., 2002. Systematic analysis of K-feldspar $^{40}\text{Ar}/^{39}\text{Ar}$ step heating results II: Relevance of laboratory argon diffusion properties to nature. *Geochimica et Cosmochimica Acta* 66, 1237–1255.
- Ludwig, K., 2009. User's Manual for Isoplot 3.70 A geochronological toolkit for Microsoft Excel. Berkeley Geochronology Center Special Publication, 4.
- Mahon, K.I., 1996. The new "York" regression: Application of an improved statistical method to geochemistry. *International Geology Review* 38, 293–303.
- Mattington, J.M., 2005. Zircon U-Pb chemical abrasion ("CA-TIMS") method: combined annealing and multi-step partial dissolution analyses for improved precision and accuracy of zircon ages. *Chemical Geology* 220, 47–66.
- Matzel, J.E.P., Bowring, S.A., Miller, R.B., 2006. Time scales of pluton construction at differing crustal levels: Examples from the Mount Stuart and Tenpeak intrusions, North Cascades, Washington. *Geological Society of America Bulletin* 118, 1412–1430.
- McDougall, I., Harrison, T.M., 1999. Geochronology and thermochronology by the $^{40}\text{Ar}/^{39}\text{Ar}$ method. Oxford University Press, New York.
- McIntosh, W.C., Chapin, C.E., 2004. Geochronology of the central Colorado volcanic field. *New Mexico Bureau of Geology and Mineral Resources Bulletin* 160, 205–238.
- McIntosh, W.C., Heizler, M., Peters, L., Esser, R., 2003. $^{40}\text{Ar}/^{39}\text{Ar}$ Geochronology at the New Mexico Bureau of Geology and Mineral Resources. New Mexico Bureau of Geology and Mineral Resources, Open file report OF-Ar-1.
- Meyer, J., Foland, K.A., 1991. Magmatic-tectonic interaction during early Rio Grande rift extension at Questa, New Mexico. *Geological Society of America Bulletin* 103, 993–1,006.
- Michel, J., Baumgartner, L., Putlitz, B., Schaltegger, U., Ovtcharova, M., 2008. Incremental growth of the Patagonian Torres del Paine laccolith over 90 k.y. *Geology* 36, 459–462.

- Miller, C.F., Miller, J.S., 2002. Contrasting stratified plutons exposed in tilt blocks, Eldorado Mountains, Colorado River Rift, NV, USA. *Lithos* 61, 209–224.
- Miller, C.F., Wark, D.A., 2008. Supervolcanoes and their explosive supereruptions. *Elements* 4, 11–16.
- Miller, C.F., McDowell, S.M., Mapes, R.W., 2003. Hot and cold granites? Implications of zircon saturation temperature and preservation of inheritance. *Geology* 31, 529–532.
- Miller, J.S., Matzel, J.E.P., Miller, C.F., Burgess, S.D., Miller, R.B., 2007. Zircon growth and recycling during assembly of large composite arc plutons. *Journal of Volcanology and Geothermal Research* 167, 282–299.
- Mills, R.D., 2012. Re-evaluating plutonic/volcanic connections and igneous textures in light of incremental magma emplacement. Ph.D. Thesis, University of North Carolina, Chapel Hill, NC (USA).
- Mills, R.D., Glazner, A.F., Coleman, D.S., 2008. Comparing the compositional patterns of volcanic and plutonic rocks using the NAVDAT database. *Geochimica et Cosmochimica Acta* 72, A631.
- Min, K., Mundil, R., Renne, P.R., Ludwig, K.R., 2000. A test for systematic errors in $^{40}\text{Ar}/^{39}\text{Ar}$ geochronology through comparison with U/Pb analysis of a 1.1-Ga rhyolite. *Geochimica et Cosmochimica Acta* 64, 73–98.
- Petford, N., Cruden, A.R., McCaffrey, K.J.W., Vigneresse, J.L., 2000. Granite magma formation, transport, and emplacement in the Earth's crust. *Nature* 408, 669–673.
- Quick, J.E., Sinigoi, S., Peressini, G., Demarchi, G., Wooden, J.L., Sbisa, A., 2009. Magmatic plumbing of a large Permian caldera exposed to a depth of 25 km. *Geological Society of America Bulletin* 37, 603–606.
- Renne, P.R., Mundil, R., Balco, G., Min, K., Ludwig, K.R., 2010. Joint determination of ^{40}K decay constants and $^{40}\text{Ar}^*/^{40}\text{K}$ for the Fish Canyon sanidine standard and improved accuracy for $^{40}\text{Ar}/^{39}\text{Ar}$ geochronology. *Geochimica et Cosmochimica Acta* 74, 5349–5367.
- Roche, P.R., Druitt, T.H., 2001. Onset of caldera collapse during ignimbrite eruptions. *Earth and Planetary Science Letters* 191, 191–202.
- Cambridge, M.S., Compston, W., 1994. Mixture modeling of multi-component data sets with application to ion-probe zircon ages. *Earth and Planetary Science Letters* 128, 373–390.
- Sanders, R.E., Heizler, M.T., 2005. Extraction of MDD thermal histories from $^{40}\text{Ar}/^{39}\text{Ar}$ K-feldspar step heating data. New Mexico Bureau of Geology and Mineral Resources Open-File Report OF-AR 26.
- Seager, W.R., McCurry, M., 1988. The cogenetic Organ cauldron and batholith, south-central New Mexico: evolution of a large-volume ash flow cauldron and its source magma chamber. *Journal of Geophysical Research* 93, 4421–4433.
- Self, S., Blake, S., 2008. Consequences of explosive supereruptions. *Elements* 4, 41–46.
- Shannon, J.R., 1988. Geology of the Mount Aetna cauldron complex, Sawatch Range: Colorado. Ph.D. Thesis, Colorado School of Mines, Golden, CO, United States (USA).
- Shannon, J.R., Epis, R.C., Naeser, C.W., Obradovich, J.D., 1987. Correlation of intracaldera and outflow and an intrusive tuff dike related to the Oligocene Mount Aetna cauldron, central Colorado. In: Drexler, J.W., Larson, E.E. (Eds.), Cenozoic volcanism in the Southern Rocky Mountains revisited: Colorado School of Mines, Quarterly, 82, pp. 65–80.
- Simon, J.I., Renne, P.R., Mundil, R., 2008. Implications of pre-eruptive magmatic histories of zircons for U-Pb geochronology of silicic extrusions. *Earth and Planetary Science Letters* 266, 182–194.
- Smith, R.L., 1979. Ash-flow magmatism. *Geological Society of America Bulletin* 71, 795–842.
- Stimac, J.A., Goff, F., Counce, D., Larocque, A.C.L., Hilton, D.R., Morgenstern, U., 2004. The crater lake and hydrothermal system of Mount Pinatubo, Philippines: evolution in the decade after eruption. *Bulletin of Volcanology* 66, 149–167.
- Tappa, M.J., Coleman, D.S., Mills, R.D., Samperton, K.M., 2011. The plutonic record of a silicic ignimbrite from the Latir volcanic field, New Mexico. *Geochemistry, Geophysics, Geosystems* 12, 14.
- Theide, R.C., Bookhagan, B., Arrowsmith, J.R., Sobel, E.R., Strecker, M.R., 2004. Climatic control on rapid exhumation along the southern Himalayan Front. *Earth and Planetary Science Letters* 222, 791–806.
- Toulmin, P., Hammarstrom, J.M., 1990. Geology of the Mount Aetna volcanic center, Chaffee and Gunnison Counties, Colorado. *U.S. Geological Survey Bulletin*, 1864, p. 44.
- Tweto, O., 1979. The Rio Grande rift system in Colorado. In: Riecker, R.E. (Ed.), Rio Grande rift: Tectonics and magmatism. American Geophysical Union, Washington D.C., pp. 35–36.
- Ulmer, P., 2001. Partial melting of the mantle wedge—the role of H_2O in the genesis of mantle-derived ‘arc-related’ magmas. *Physics of the Earth and Planetary Interiors* 127, 215–232.
- Ulmer, P., Müntener, O., Kägi, R., Alonso Pérez, R., Villiger, S., 2007. Where do primitive arc magmas differentiate and acquire major and trace element composition? An assessment based on field, geochemical and experimental data: SOTA-State of the Arc Abstracts with Program.
- Vance, D., Bickle, M., Ochs-Ivy, S., Kubik, P.W., 2003. Erosion and exhumation in the Himalaya from cosmogenic isotope inventories of river sediments. *Earth and Planetary Science Letters* 206, 273–288.
- Verplanck, P.L., Farmer, G.L., McCurry, M., Mertzman, S.A., 1999. The chemical and isotopic differentiation of an epizonal magma body, Organ Needle Pluton, New Mexico. *Journal of Petrology* 40, 653–678.
- Walker, B.A., Miller, C.F., Claiborne, L.L., Wooden, J.L., Miller, J.S., 2007. Geology and geochronology of the Spirit Mountain batholith southern Nevada: Implications for timescales and physical processes of batholith construction. *Journal of Volcanology and Geophysical Research* 167, 239–262.
- White, S.M., Crisp, J.A., Spera, F.J., 2006. Long-term volumetric eruption rates and magma budgets. *Geochemistry, Geophysics, Geosystems* 7, 1–20.
- Wiebe, R.A., 1994. Silicic magma chambers as traps for basaltic magmas: The Cadillac Mountain Intrusive Complex, Mount Desert Island, Maine. *Journal of Geology* 102, 423–437.
- Wood, B.J., 2004. Melting of fertile peridotite with variable amounts of H_2O . In: Sparks, R.S.J., Hawkesworth, C.J. (Eds.), The state of the planet: Frontiers & Challenges in Geophysics. American Geophysical Union, Washington D.C., pp. 69–80.
- Zimmerer, M.J., McIntosh, W.C., 2012. The geochronology of volcanic and plutonic rocks at the Questa caldera: constraints on the origin of caldera-related silicic magmas. *Geological Society of America Bulletin* 124, 1394–1408.